WYLE LABORATORIES
TESTING DIVISION, HUNTSVILLE FACILITY

WYLE LABORATORIES - RESEARCH STAFF

REPORT WR 68-13

STATIC AND RELATIVE FLUCTUATING PRESSURE RESULTS OF A WIND TUNNEL INVESTIGATION OF SUBSONIC AND SUPERSONIC SEPARATED FLOW ABOUT CYLINDRICAL AND SATURN V MODEL PROTUBERANCES

By

S. Dendrinos, Jr.

Work Performed Under Contract No. NAS8-21026

Principal Investigator - J.E. Robertson

June 1968

WYLE LABORATORIES
RESEARCH STAFF
Huntsville Facility Huntsville, Alabama

COPY NO. 6

SUMMARY

Shadowgraph, pressure, and flow visualization experiments were performed on a series of cylindrical and two scale model Saturn V protuberances in the MSFC's 14- by 14-in. Wind Tunnel. The objective was to define the mean flow and acoustic environments around various protuberances, at both transonic and low supersonic Mach numbers. The results generally support earlier analysis of the flow. The flow region around the base of cylindrical protuberances was found to be three-dimensional. Upstream separation data was collapsed by the assumption that normalized height to the normalized diameter was proportional to the tangent of a characteristic separation shock wave angle, which varies with Mach number. Using this approach, it is possible to predict separation from Mach 1.96 to 5.0 for any protuberance in a crossflow. The magnitude of the overall acoustic environment in the protuberance wake was found to be 8 to 10 dB relative to the undisturbed flow over the model at transonic speeds.

TABLE OF CONTENTS

		Page
SUMMARY		ii
TABLE OF CONTENTS		iii
LIST OF TABLES		iv
LIST OF FIGURES		v
LIST OF SYMBOLS		viii
1.0	INTRODUCTION	1
1.1	Background	1
1.2	Objective	1
2.0	APPARATUS AND TESTS	2
2.1	Test Requirements	2
2.2	Wind Tunnel Description	2
2.3	Test Specimens	2
2.4	Splitter Plate	2
2.5	Wind Tunnel Test Conditions	3
2.6	Instrumentation	3
2.7	Flow Visualization	4
3.0	RESULTS AND DISCUSSION	5
3.1	Clean Model Flow Characteristics	5
3.2	Supersonic Speeds	6
3.3	Transonic Speeds	7
3.4	Acoustic Environment	8
4.0	ANALYSIS	10
4.1	Supersonic Separated Flows	10
4.2	Transonic Separated Flows	14
4.3	Similarities between Two-and Three-Dimensional Protuberance Flows	15
5.0	CONCLUSIONS	17
REFERENCES		19
ACKNOWLEDGEMENTS		21

LIST OF TABLES

Table		Page
I	Wind Tunnel Test Conditions	22
II	Protuberance Configuration	27
III	Summary of Current Data Obtained at Mach 1.96	28
IV	Measured Acoustic Environment - Overall Sound Pressure Level In Decibels	29
V	Increase in Acoustic Environment due to Protuberances - Presented as Decibels Where $\Delta dB = OSPL_{Protuberance} - OSPL_{Clean\ Plate}$	33

LIST OF FIGURES

Figure		Page
1	Photograph of the MSFC 14- by 14-Inch Trisonic Wind Tunnel	37
2	Photograph of Test Specimens	38
3	Photograph of Boundary Layer Rake Installed on the Splitter Plate, Which is Mounted in the Wind Tunnel	39
4	Splitter Plate Mounted in the MSFC 14- by 14-Inch Transonic Wind Tunnel	40
5	Measurement Locations for Model Splitter Plate	41
6	Pressure Profile from Boundary Layer Rake.	42
7	Shadowgraphs of Clean Plate with Grit Near the Leading Edge	43
8	Shadowgraphs of Clean Plate Without Grit	44
9	Pressure Profile Down the Centerline of the Splitter Plate - Clean Configuration	45
10	Upstream Centerline Pressure Profile for Cylindrical Protuberanct at Mach 1.96	46
11	Shadowgraphs of 1-Inch Cylinder at Mach 1.96	47
12	Shadowgraph of 1-Inch Cylinder at Mach 1.96 and Height = 1.0 Inch	48
13	Shadowgraph of 1-Inch Cylinder at Mach 1.96 and Height = 2.0 Inches	49
14	Shadowgraph of 2-Inch Cylinder at Mach 1.96	50
15	Correlation of Normalized Height with Normalized Separation Length for Cylindrical Protuberances at Mach 1.96	51
16	Shadowgraphs of the Saturn V Model Protuberances at Mach 1.96	52
17	Oil Flow Photographs of Cylindrical Protuberances at Mach 1.96	53
18	Composite Conception of Infinite Cylinder Wake Region	54
19	Downstream Centerline Pressure Profile for Cylindrical Protuberances at Mach 1.96	55

LIST OF FIGURES (Continued)

Figure		Page
20	Upstream and Downstream Pressure Distribution of a 1-Inch Cylinder	56
21	Shadowgraphs of Protuberances at Mach .80	57
22	Shadowgraphs of Protuberances at Mach .90	58
23	Shadowgraphs of Protuberances at M = 1.15	59
24	Oil Flow Photograph of a Cylinder Where H = 1.0, D = 1.0	60
25	Normalized Height versus Normalized Separation Length for Cylinders	61
26	Centerline Fluctuating Pressure Profile Upstream and Downstream of Cylindrical Protuberances at M = .80, .90, 1.15, and 1.96	62
27	The Variation of Separation Shock Angle with Mach Number - Schlieren - Shadowgraph Data	63
28	Idealized Model of Separation Upstream of a Cylindrical Protuberance at M = 2.5 and $\theta = 30^{\circ}$	64
29	Correlation of Flow Fields and Stagnation Pressure (Miller Reference 13)	65
30	Bow Shock Standoff Distance versus Mach Number for an Infinite Cylinder	66
31	Correlation of Normalized Height with Normalized Separation Length for Cylindrical Protuberances at Mach 2.2, 2.7, and 5.0	67
32	Variation of Vertical Intercept (-B) with Mach Number	68
33	Modified Idealized Model of Separation Upstream of a Cylindrical Protuberance at M = 2.5, $\theta = 30^{\circ}$	69
34	A Series of Curves Presenting Separation Length and Height as a Function of Mach Number	70
35	Expected Shock System Upstream of a Tall Protuberance at Low Supersonic Mach Numbers	71
36	Comparison of Upstream Centerline Pressure Profile with the Lambda Shock System	72

LIST OF FIGURES (Continued)

Figure		Page
37	Upstream Centerline Pressure Profile for Cylindrical Protuberances	73
38	Correlation of Height and Separation Length for Two-Dimensional 90° Steps (Lowson Reference 17)	74
39	Photograph of Two-Dimensional Flow Showing Separation Upstream of a 90° Step. M = 2.49, Step Height = .6 Inches, (Lowson Reference 17)	75

LIST OF SYMBOLS

B	vertical intercept in diameters
C_p	pressure coefficient $\frac{P - P\infty}{Q\infty}$
D	cylinder diameter
L_s	separation length - inches
H	cylinder height - inches
P_o	wind tunnel stagnation pressure - psig
P	splitter plate pressure - psia
Q	dynamic pressure (psi)
R_L	Reynolds number/ft.
OSPL	overall sound pressure level in decibels re: 2×10^{-5} n/m^2
T	temperature F^o
X	distance from protuberance
ΔdB	(OSPL protuberance - OSPL clean plate) = in decibels
δ	nominal boundary layer thickness - inches
δ_w	two dimensional separation angle - degrees
θ	separation shock wave angle - degrees
σ	three dimensional conical separation shock angle - degrees
o	stagnation line
∞	free stream

1.0 INTRODUCTION

1.1 Background

Protuberances have an infinite number of possible geometries so that a general discussion of the flow field is difficult. For example, the Saturn V alone has approximately 75 individual protuberances which include reaction control rockets, auxiliary propulsion systems, vents, tunnels, etc. (Reference 1). Each protuberance generates its own flow field which may interact with the external flow field already present and lead to the imposition of large steady and fluctuating loads on both the protuberance and the surrounding structure. It is obviously impractical to investigate the environment of every protuberance, which may be attached to the external surface of a launch vehicle, especially if some general features of the flow can be defined from a systematic study involving generalized protuberance geometries.

Dendrinos (Reference 2) presented a systematic study of protuberances in supersonic flows from a comprehensive literature survey. In this study, the upstream separation was found to be three-dimensional and a technique was presented for predicting the oblique separation shock angle and the separation length upstream of the protuberance. The variation of oblique separation shock angle with Mach number was predicted by the assumption of a three-dimensional conical shock with a constant 17-degree semi-vertex separation angle. The geometry of separation upstream of protuberances was related to the conical separation shock wave and was shown to be hyperbolic. This hyperbolic flow separation was found to pertain to flared protuberances as well as 90-degree protuberances.

A future test program is being contemplated in which the Propulsion Wind Tunnel, Sixteen-foot transonic (16T) at the Arnold Engineering Development Center (AEDC), will be used as a test facility to investigate fluctuating pressures around cylindrical protuberances mounted on a splitter plate.

1.2 Objective

The objective of the present study was to perform wind tunnel tests to define the mean flows around various model cylindrical protuberances, and to acquire data on the relative magnitude of the acoustic environment around protuberances at both transonic and supersonic Mach numbers.

The supersonic portion of this test should verify and extend the prediction technique of Reference 2 to lower Mach numbers.

Four percent models of the Auxiliary Propulsion Unit (APU) and the Rocket Control System (RCS) protuberances were also tested to provide data which could be used to correlate specific protuberance geometries with the generalized cylindrical protuberances.

2.0 APPARATUS AND TESTS

2.1 Test Requirements

Test requirements were outlined in Reference 3. Inevitably, changes to the run schedule were made and the actual run schedule is shown in Table I.

2.2 Wind Tunnel Description

George C. Marshall Space Flight Center's (MSFC) wind tunnel was utilized. The tunnel is an intermittent trisonic blowdown tunnel operated from pressure storage to vacuum or atmospheric exhaust (Figure 1). The test section measures 14 by 14 by 20 inches in each of the two interchangeable test sections. The transonic section permits testing at Mach numbers of .2 to 2.5. The walls of the transonic section are perforated walls with 5/32" diameter holes which are slanted at 30 degrees with respect to the flow direction. The porosity of the walls is varied by the use of a double wall arrangement. Air is supplied to a 6000-foot storage tank at approximately 40° F dew point and 500 psi. The compressor is a three-stage reciprocating unit driven by a 1500 hp motor.

The tunnel flow is established and controlled with a servo-actuated gate valve. The controlled air flows through the valve diffuser into the stilling chamber and heat exchanger where the air temperature can be controlled from ambient to approximately 180° F. The air then passes through the test section which contains the nozzle blocks and the test region. The supersonic diffuser has movable floor and ceiling panels which are the primary means of controlling the subsonic Mach numbers and permit more efficient running at supersonic Mach numbers. Tunnel flow is exhausted through an acoustically damped tower to atmosphere or into a vacuum field of 42,000 cubic feet. The vacuum tanks are evacuated by pumps driven by a total of 500 hp. A more complete description of this facility, and the latest calibration results are presented in Reference 4.

2.3 Test Specimens

A photograph of the test specimens is given in Figure 2. The cylindrical specimens ranged from .25 to 2 in. in diameter and had height to diameter ratios ranging from .25 to 2.0. The RCS and APU protuberances are four-percent models of those detailed in Reference 1.

2.4 Splitter Plate

The tests were made using the splitter plate shown in Figure 3. The plate was constructed from 1.25 inches thick aluminum and was 20.6 in. long by 5.25 in. wide. The width-wise portion of the plate was curved to a radius of 9.37 inches. In order to prevent blockage, the plate was mounted on legs which attached to the side and positioned such that the stream-wise centerline of the plate was 5.1 inches from the

tunnel floor. A .25-inch wide boundary layer trip made of 36-grit was mounted on the test surface .25-inches downstream of the leading edge. The grit was not utilized on the Mach 1.96 runs except inadvertently during the oil flow portion of the tests. The splitter plate position in the wind tunnel is detailed in Figure 4. (Wyle Drawing No. D-68840).

2.5 Wind Tunnel Test Conditions

The test was conducted at Nominal Mach numbers of .80, .90, 1.15 and 1.96. The top surface of the splitter plate was at zero angle of attack. Table I contains the test conditions for each run. The tunnel stagnation temperature was held constant at 100° F while the stagnation pressure was varied from 7 psi g at Mach numbers 0.80, 0.90, and 1.15 to 15 psi g at Mach number 1.96. Table II is given as a guide to configuration numbers utilized in photographs and other data. The tunnel walls were operated at maximum porosity.

2.6 Instrumentation

2.6.1 Static Pressure

Eighty-four static pressure orifices were located on the splitter plate model, see Figure 5 (Wyle Drawing No. D-67735). All orifices were .040 inches in diameter and were constructed of 1/16-inch stainless steel tubing which was inserted into the splitter plate surface such that the orifice end of the tubing was flush and perpendicular to this surface. The stainless steel tubing for each orifice extended for approximately one foot and was connected to a system of pressure scanning switches (Scanivalves) mounted outside the tunnel by approximately four to five feet of plastic pressure tubing. Each Scanivalve was capable of scanning eleven pressures and consisted of a standard half-inch flush-diaphram, strain gage transducer rated at 12.5 psid. A 0.5 second delay time was utilized between successive scans of each Scanivalve in order to ensure that line transients were negligible.

Data from each Scanivalve was recorded by a solid state digital data acquisition system and transferred to punched cards during each run. This data was later reduced by a computer to proper coefficient form and outputted in the form of punched cards and line printer listings.

2.6.2 Fluctuating Pressure System

The acoustic environment was measured by six microphones flush mounted to the external surface of the splitter plate (see Figure 5). The acoustic measuring system consisted of a Kistler 601L, 5/32-inch diameter microphone, a Kistler 553-A charge Amplifier, and an Ampex-1200, fourteen-channel tape recorder. In general the microphone and charge amplifier was connected by a two-foot cable to the microphone. The acoustical data was recorded to each run and then played back between runs and reduced through a Ballentine 320 true RMS voltmeter, to overall sound

pressure level. Channels 1, 2, 3, 4, 5, 7 and 8 of the recorder were utilized for acoustic data purposes. The calibration for microphones 1 and 2, to an input of 160 dB SPL was an output voltage of 295 mv and 276 mv respectively. When subjected to 160 dB SPL input, microphones 3 through 6 gave an output of 316 mv. When the data was reduced to Overall Sound Pressure Level (OSPL), the calibration utilized for all channels was 316 mv = 160 dB, thus data from microphones 1 and 2 can be corrected by the addition of .58 and 1.13 decibels respectively.

2.7 Flow Visualization

Flow visualization was accomplished by both shadowgraph and oil flow techniques.

The shadowgraphs were recorded on 10 in. by 20 in. high speed black and white film, with approximately 1.5 X magnification. The shadowgraphs taken at Mach numbers .80, .90 and 1.15 were taken with the light source slightly higher than the model. For the Mach 1.96 runs, the light source was on the same level as the top of the splitter plate so that the magnification was slightly larger than 1.5 X in these shadowgraphs. The shadowgraph, which is proportional to the second derivative of the flow density, was chosen because it appeared to give greater resolution of boundary layer separation.

The oil flow studies were performed by spraying china clay on the splitter plate surface, letting it dry, and then spraying oil of wintergreen over the china clay. The wind tunnel was then started and test conditions held constant until the oil evaporated sufficiently to allow the flow pattern to be frozen on the plate by the china clay. The flow patterns were not completely defined for all cases due to the variation in the amount of oil sprayed on the plate, the variation in the run time and possible effects of stopping transients.

The flow patterns could not be photographed while the tunnel was running. Further difficulties were encountered in producing high quality photographs in that the splitter plate could not be removed from the tunnel and a restricted field of view resulted in the loss of detail in the oil flow photographs.

3.0 RESULTS AND DISCUSSION

3.1 Clean Model Flow Characteristics

Certain general remarks concerning all tests are in order at this point. First,it should be noted that the shadowgraphs were made with glass walls on two sides, while the pressure data were acquired with all walls being porous. Thus,it may be possible that the flow conditions for the shadowgraph study were altered from the flow conditions for the pressure study. Grit was placed near the leading edge to ensure that a thick turbulent boundary layer was established. At the onset of testing, it was feared that the secondary flow beneath the splitter plate may have been choked. This was checked by measuring the total and the static pressure in the secondary flow. At a free-stream Mach number of 0.80, the local Mach number under the splitter plate was found to be 0.82 showing no blockage, whereas,at a free-stream Mach number of 0.90 a little blockage was present as the local Mach number under the plate was 0.82. Blockage increased at a free-stream Mach number of 1.15, as the local Mach number under the plate was found to be 0.89.

A boundary layer rake was installed 6.2 inches downstream from the leading edge and is shown in Figure 3. The impact-pressure profiles from the rake tests are given in Figure 6. It is apparent from this figure that the use of grit does not make a significant change in boundary layer thickness over the no-grit condition at subsonic Mach numbers. This effect may be explained by referring to the shadowgraphs of the boundary layer on the clean plate configuration presented in Figures 7 and 8. In Figures 7a and 8a there appears to be separation occurring near the leading edge of the splitter plate. The smooth centerline pressure profile shown in Figure 9, argues that reattachment must occur shortly after separation. This apparent separation reattachment phenomenon about the leading edge has one undesirable side effect, namely a thickened boundary layer in unequilibrium. Also, since local separation appeared to have occurred in the vicinity of the grit, the effect of the grit on the boundary layer thickness would be negligible.

The centerline pressure distributions at Mach 1.15 experienced larger variations due to the presence of shock waves standing on the splitter plate. Thus, data at this Mach number will have to be virtually ignored as the standing shocks on the splitter plate interfere with the effects of protuberances.

The boundary layer thickness for the data to be presented in this report is:

Mach	δ	Source
0.80	0.98 inches	Rake Pressure Profile
0.90	0.90 inches	Rake Pressure Profile
1.15	(0.28 - 0.40) inches*	Rake Pressure Profile
1.96	(0.10) inches*	Shadowgraph

* Uncertainty in measurement

An effort was made to investigate methods for achieving a thinner boundary layer at subsonic Mach numbers. It was proposed to position the splitter plate so that the leading edge would be at a negative angle of attack. Because of limitations of time, this proposal could not be carried out, however, it was possible to raise that portion of the tunnel floor on which the splitter plate was attached by 2.5°. This had the effect of placing the splitter plate on a 2.5° ramp. This condition clearly reduced the boundary layer on the splitter plate from .98 inches to .70 inches at Mach 0.80 and from .90 to .80 inches at Mach 0.90.

3.2 Supersonic Speeds

3.2.1 Upstream Separation

Separation lengths were determined from the pressure data by assuming separation occurred where there was a significant pressure rise above free stream pressure. The spacing of the pressure instrumentation, while it did not allow complete definition of the inflection point in the vicinity of separation, was useful in defining the overall pressure profile upstream of the various protuberances, see Figure 10.

Separation lengths were determined directly from the shadowgraphs in Figures 11-14 by extending the separation shock line below the boundary layer to the splitter plate. The centerline portion of the oil flow photographs were utilized for obtaining separation length.

The separation shock angle was found from the shadowgraph to be a nominal 40°. The correlation between protuberance height and separation length obtained from pressure, shadowgraph and oil flow results is presented in Figure 15. As is evident, the agreement between the three data sources is excellent. The slope of the correlation line is found to be the tangent of 40° and the vertical intercepts B is -0.47. As the H/D ratio exceeds 1.0 it appears that the separation length might approach a constant. A summary of the Mach 1.96 separation data is presented in Table III. The agreement between pressure and shadowgraph data given in Figure 15 shows that accurate determination of the upstream separation can be accomplished provided that the instrumentation density is sufficient.

The shadowgraph of the RCS motors shown in Figure 16a, shows that the upstream motor has a strong detached bow shock with a weak separation shock. The reason for this type of shock structure can be attributed to the configuration of the RCS motors. The upstream motor is suspended above the vehicle so that the motor acts as a blunt body mounted on a string. The motors perpendicular to the streamwise direction also act as blunt bodies, however, because of the smaller frontal area presented to flow, the detached bow shocks generated about them are proportionately smaller.

A strong shock wave is shown attached to the front of the APU in the compression corner, see Figure 16b, and as might be expected, very little evidence of separation

is found due to the shallow flare angle of the protuberance. This is in substantial agreement with the work of Price et al., (Reference 12) which was performed at Mach 4.44.

3.2.2 Wake Flow Patterns

Oil flow studies were conducted in order to increase the visualization of the flow patterns around the protuberances and the results are presented in Figure 17. The patterns near the side of the model for the two-inch protuberance are questionable due to the size of the protuberance relative to the splitter plate. However, as was seen in Figure 15, the upstream separation lengths measured from the oil flow photographs are in good agreement with pressure data.

A composite conception of the wake region behind an infinite cylinder is shown in Figure 18. As can be seen, the wake necks down at a distance of approximately one diameter downstream of the cylinder. The region between the cylinder and the wake neck appears to be one of low energy and separated flow. The downstream centerline pressure profile for various height cylinders is given in Figure 19. The static pressure immediately downstream of the cylinder is relatively low and returns to free-stream conditions at a longitudinal distance which ranges from .75 to 2.5 for a variation of height to diameter ratio ranging from .25 to 2.0. It is expected that as the H/D ratio exceeds 2.0 the necking of the wake should occur at a constant longitudinal distance downstream of the cylinder. It must be understood, however, that the wake region of the infinite cylinder is affected only by the standoff bow shock, while the wake region of finite cylinder on a plate is affected by the interaction of both the separation shock and standoff shock system which occurs upstream of the cylinder. The flow patterns from the oil flow studies are in substantial agreement with the pressure data and even show some signs of the trailing shock phenomena that is characteristic of the infinite cylinder. The quantity and resolution of this data does not permit a more complete analysis of the wake at this time.

Because of restriction of testing time, the oil flow studies for the APU and RCS motors protuberances were not performed at Mach 1.96.

3.3 Transonic Speeds

3.3.1 Upstream Separation

The centerline pressure distribution upstream and downstream of a one inch cylinder at Mach 0.80 and Mach 0.90 is shown in Figure 20. The pressure profile upstream of the protuberance at Mach 0.8 and 0.9 shows a very gradual rise compared to the supersonic case where there is peak a dip and a sharp rise in pressure. Also in the transonic case, the magnitude of the pressure is significantly smaller. Shadowgraphs of the three types of protuberances is given in Figures 21-23, while the oil flow flow photographs are given in Figure 24. Since there was a similarity in the upstream pressure profiles and gradients for various cylindrical protuberances, it was concluded

that separation should occur for similar rises in pressure. Thus, a pressure rise P/P_∞ of 1.04 was assumed to be sufficient to cause separation. This assumed pressure rise gave good correlation with the oil flow results and if it is not exactly the correct pressure, it at least points out the separation trend with variation in protuberance configuration. The unequilibrium boundary layer also may give rise to a larger separation length than a normal boundary layer, since the unequilibrium boundary layer is easier to separate. The normalized separation length versus normalized heights is presented in Figure 25, for Mach .8 and .9 cases respectively. There appears to be a strong correlation between height and separation length which parallels somewhat the results found supersonically. As the height to diameter ratio exceeded one, it was expected that the separation length would approach a constant. This does not appear to have happened due possibly to the thick boundary layer which is approximately one inch in thickness. A median line drawn through the data in the Mach .8 and .9 case appears to make an angle of 28 degrees.

At Mach .8, a weak shock wave is evident on the shoulder of the APU protuberance which apparently results from a local supersonic flow region. At Mach .9, a shock wave is found on the splitter plate near the leading edge. There are characteristic standing shock patterns on all of the shadowgraphs taken at Mach 1.15. However, the one-inch cylinder shown in Figure 23a, does have a nearly normal shock wave standing off from the cylinder. There is obviously some question as to whether this is a real effect or results from flow blockage on the splitter plate at that Mach number. A weak shock wave appears to be attempting to attach itself to the compression corner in front of the APU at $M_\infty = 1.15$ as shown in Figure 23c.

The oil flow photographs at Mach 1.15 are included for comparison purposes even though the accuracy of this data is questionable. The Mach .8 and .9 oil flow patterns show a form of upstream separation not unlike that which occurs supersonically.

3.3.2 Wake Flow Patterns

The wake patterns are not well defined in the oil flow photographs of Figure 24, however, there is enough resolution to see that the wake pattern transonically differs from the supersonic case. The centerline pressure profile downstream of a cylinder presented in Figures 20 a and 20 b shows that the length of the low pressure region is strongly related to the protuberance height; however, this effect could be due to the thickness of the boundary layer.

3.4 Acoustic Environment

The acoustic data taken from the microphones was the overall sound pressure level in decibels. Because the locations of the microphones were fixed while the protuberances were varied in height, and diameter, data could be found up to 3.5 diameters upstream and 4.25 diameters downstream of the cylindrical protuberances. This data was taken along the streamwise centerline of the protuberances. Because of a high background noise of the tunnel, and because the effect of the protuberance on

the acoustic environment was required, the acoustic data was normalized by dividing the protuberant pressures by the pressure taken on the clean plate. In terms of decibels, this consisted of subtracting the overall sound pressure level of a microphone when the splitter plate was clean from the overall sound pressure level of it when a protuberance was on the plate. This difference in decibels, ΔdB, was plotted for a variation of height and Mach number. Figure 26 is provided as a guide for the expected rise in Sound Pressure Level on a plate due to the addition of Protuberances. It is evident from the sparse data that the increase in the acoustic environment occurs near the protuberance and can, in some cases, exceed 6 dB at transonic speeds and 12 dB at supersonic speeds.

One significant pattern which appeared in this data was the increase in the acoustic environment in the wake of the cylinders appears to remain at a high level (6 dB) for a H/D = 1.0 for at least two diameters downstream of the cylinder at transonic speeds.

The P/q values for the clean configurations of the splitter plate rangea from .05 at Mach ∞ = .80, to .03 at M ∞ = 1.96.

4.0 ANALYSIS

While the test results are of practical value, their use is limited to the flow conditions under which they were obtained. An analytical method of predicting upstream separation is desirable, preferably one which would apply generally to the regime of transonic and supersonic flows with turbulent boundary layers.

4.1 Supersonic Separated Flows

In Reference 2, it was shown that supersonic flow around protuberances was three dimensional and a method for collapsing the data was presented for Mach numbers ranging from 2.7 to 5.0. Combining the data of Reference 2 and the data from the present tests, an ideal model of protuberance separation was developed.

It was noticed in the literature survey and in the present tests that the angle of the oblique separation shock was constant for a given Mach number even though the cylindrical protuberances were varied in height and diameter. This agrees substantially with the free interaction hypothesis advanced by Chapman, Khuen, and Larson (Reference 19), for two-dimensional flows. This would indicate that there was a characteristic separation shock angle associated with Mach number that was independent of protuberance geometry. It was found in Reference 2 that the variation of separation shock angle with Mach number for the limited data in the survey could be predicted by assuming conical flow and a constant separation angle of 17 degrees using the tables of Reference 5. Since this time, additional data (References 6-14) have become available and pertinent results from these references are shown in Figure 27. These data were obtained exclusively from Schlieren photographs and shadowgraphs and represents the nominal separation shock angles where there was an abundance of data. In the Mach number range 2.5 to 5.0, the constant separation angle $\sigma = 22$ degrees gives a better fit. This variation in separation angle does not in any way violate the assumption that there exists a characteristic separation shock angle at a given Mach number, however, it does mean that it may not be possible to predict this shock angle from one constant separation angle over a large Mach number range.

It is obvious that for three-dimensional protuberances, there exists circumferential flow about the protuberance, such that any upstream three-dimensional shock wave will not only approach the protuberance but will bend around it, in a sense conforming to the protuberance shape. The detached bow shock in front of infinite cylinders is a well known example of a shock wave structure which is influenced by protuberance shape. Since the separation shock angle for a given Mach number is constant, even though the height and diameter of a protuberance may vary, then there should be a method of predicting separation length. An idealized model was proposed in Reference 2 which would correlate height and separation length, see Figure 28. If the height and separation length are normalized by protuberance diameter, then the relationship between height and separation length is given by

$$\frac{\frac{H}{D}}{\frac{L_s}{D}} \approx \text{Tan } \theta \qquad (1)$$

where θ is the separation shock wave angle.

This idealized model promises to be a valuable means of predicting the separation length upstream of a cylinder, where only the Mach number and cylinder dimensions are known.

The actual case taken from Miller (Reference 13) is shown in Figure 29. It was found that when a protuberance was short relative to the boundary layer thickness the boundary layer passes over, or around the obstacle without a general change in character. As the protuberance height approaches or exceeds the nominal boundary layer thickness, the flow pattern changes markedly. The boundary layer cannot overcome the adverse pressure gradient caused by the obstacle and therefore separates from the plate. This separation is accomplished by an oblique separation shock which was mentioned earlier. This shock wave may pass above intermediate length cylinders, but when the H/D ratio exceeds 1.0 the separation shock intersects the cylinder bow shock. This results in a lambda-shaped shock wave configuration. The bow shock in the central region is dominated by two-dimensional flow. Amick (Reference 15) and others have found that the distance the bow shock stands off from an infinite cylinder is dependent on Mach number such that:

$$S = .19 + \frac{1.2}{M^2 - 1} + \frac{0.7}{(M^2 - 1)^2} \qquad (2)$$

where S is the standoff distance in diameters Figure 30 is a plot of this variation of standoff distance with Mach number.

It is to be expected that as the Mach number approaches 1.0, the bow shock should exert an influence on the separation shock and indirectly to the separation length.

The correlation of normalized height to separation length plotted from the current data as well as the data of Lucero, Walthup, Halprin and Westkemper (References 7, 8, 10 and 14) respectively result in lines which do not pass through the origin (See Figures 15, 31). This results in the correction of Equation (1) such that:

$$\frac{\frac{H}{D} - B}{\frac{L_s}{D}} = \text{Tan } \theta \qquad (3)$$

where B is the vertical intercept.

The vertical intercepts found in the aforementioned figures are negative and vary with Mach number. The physical interpretation of this is that the bow shock holds the separation shock away from the cylinder thereby increasing the separation length from what one might have expected from the idealized model in Figure 28 and Equation (1). If this is the case, then a plot of the standoff distances compared to the vertical intercepts should result in good correlation. The correlation results in a straight line where:

$$B = -0.818\ S + .079 \qquad (4)$$

Combining equations (2) and (4) the vertical intercept B can be expressed as a function of Mach number such as:

$$-B = .071 + \frac{1.14}{M^2 - 1} + \frac{0.573}{(M^2 - 1)^2} \qquad (5)$$

Figure 32 is a plot of the variation of the vertical intercept B with Mach number.

The proposed idealized model for determining separation length is then modified include the effects of the bow shock standoff distance and would appear as is given in Figure 33. Combining Equations (3) and (5) produces an equation for predicting separation length which includes bow shock influence.

$$L_s = \frac{\frac{H}{D} + .071 + \frac{1.14}{M^2 - 1} + \frac{0.573}{(M^2 - 1)^2}}{\text{Tan } \theta} \qquad (6)$$

where θ is the separation shock angles given in Figure 27.

A series of curves are given in Figure 34 for the predicted correlation between height and separation length from Mach 2 to Mach 5, using Equation (6). Above Mach 5, the bow shock standoff should be sufficiently small so that Equation (1) can be utilized.

For the present analysis as H/D becomes greater than one, it is assumed that the separation length becomes a constant. In the H/D range between 1 and 3 or possibly higher depending on the bow shock standoff distance, the separation length is affected by the curvature of the bow shock and therefore may vary slightly. Because of the limited data available for these intermediate height protuberances this effect cannot be exactly defined at this time and is left for future studies when this data might be available.

4.1.1 The Special Case of Low Supersonic Separated Flow

The Mach number range between 1.0 and 2.0 shall be referred to as a special case of low supersonic separated flow due to the complexities of the flow in this range.

The separation shock angle varies from 90 to 35 degrees in this Mach number range, while the bow shock standoff distance may vary from $+\infty$ to .45 diameters. Adding to the complexity of the flow is the mutual interaction of the separation shock with the bow shock, which is nearly normal.

In order to understand the magnitude of the problem, Equation (6) was utilized in constructing an expected upstream lambda shock system, (See Figure 35). It is quickly evident that as the separation shock angle θ approaches the bow shock angle the lambda shock system will coalesce into one shock, which is nearly normal. (One of the effects of this bow-shock-separation shock interaction might be a larger separation wave angle than would be predicted by a constant $\sigma = 22$ degrees.

At this time, only approximations of the flow in this restricted Mach number range can be made. It is hoped that a comprehensive set of tests in AEDC's 16T tunnel will unravel the complex flow occurring in this Mach number range, as most Saturn Vehicles experience maximum dynamic pressures at a Mach number of approximately 1.4.

4.1.2 Upstream Pressure Distribution

The upstream centerline plate pressure profile is correlated to the lambda shock system, (see Figure 36). It can be seen that the ratio of local pressure to free-stream pressure is approximately 1.0 prior to separation. A sharp pressure rise occurs at separation. This pressure rise or first disturbance is taken at the point where the boundary layer separates. The limited number of pressure orifices, however, did not permit a full definition of the inflection point in the pressure rise. The pressure profile between 1.5 and .25 diameters decreases in pressure. This dip in pressure is most likely related to a reverse flow region. The pressure rise from .25 diameters to the cylinder is very sharp. This pressure rise can be attributed to a stagnation region near the root of the cylinder and the influence of the second leg of the lambda shock system on this stagnation region. In Figure 29 the influence of the bow shock on the cylinder stagnation pressure was presented. It was obvious that the shape of the shock influenced the stagnation pressure profile.

Similarity in pressure profile from other sources, and the present results are shown in Figure 37. An upstream pressure profile to Mach 4.44 is given in Figure 37d. One feature that is outstanding in these pressure profiles is that the first peak occurs at a P/P_∞ ratio of 2.0 for a variety of Mach numbers. This could be a significant trend, however, the small amount of data obtained gives rise to uncertainty at this time.

4.2 Transonic Separated Flows

The whole field of transonic separated flows about protuberances is virtually unexplored. There have been numerous studies of drag about cylinders in transonic flow which have been summarized by Goldstein (Reference 16).

In the case of supersonic flow, it was relatively easy to comprehend the mechanism of separation. The adverse pressure gradient caused by protuberance flow blockage resulted in an oblique separation shock. Because the flow, including the three-dimensional separation shock system, more or less hugs the protuberance, the separation length was determined by the separation angle and the height of the protuberance. In transonic flow by comparison no shocks are generated, therefore, it is expected that the separation phenomenon is dependent on protuberance configuration i.e., diameter and height.

In the upstream pressure profiles of Figure 20, it is observed that the pressure rise is gradual reaching a peak very close to the cylinder. There is a pressure rise which can be assumed to induce separation and this pressure rise does vary with protuberance height and diameter. The height to diameter ratio exerts a strong influence on the wake flows downstream of the cylinders with the length of the low pressure region being greater for tall protuberances than shorter ones. Pressure in the immediate vicinity of the protuberance decreased with increasing height to diameter ratio.

The correlation between height and separation length for the protuberances on a Mach .8 and .9 flow results in the correlation lines shown in Figure 25.

The normalized separation length is then given by the expression:

$$\frac{L_s}{D} = \frac{\frac{H}{D} + .38}{.53} \tag{7}$$

In our present tests, the separation length did not approach a constant after the H/D ratio became greater than one, as expected. This effect is due possibly to the thickened boundary layer which was one inch while the protuberance height in one case was 2.0 inches. This boundary layer effect is left as a subject for further study in the large scale test to be performed at AEDC.

4.3 Similarities between Two-and Three-Dimensional Protuberance Flows

Two-Dimensional (2D) protuberances have been studied more extensively than Three-Dimensional (3D) protuberances, due to the ease with which 2D flow can be expressed. A comparison of separation in front of these two types of protuberances will be made in order to explore the possibility of a unifying explanation for the separation phenomena.

In the supersonic flow a protuberance causes an upstream shock to form. When the flow encounters a sufficient adverse pressure gradient through the shock wave, the low momentum fluid in the boundary layer is brought to rest and the boundary layer separates.

In the 3D case, the separation shock is a three-dimensional conical shock wave which folds itself around the shape of the protuberance, conforming to the protuberance shape in the vicinity of the protuberance. Thus, the separation length is a direct function of the separation angle and protuberance height.

In the two-dimensional case, there is no side relief or circumferential flow and the separated shear layer must pass over the top of the protuberance. (As a result the separation length is determined approximately by the separation angle and protuberance height). The general equations for separation are then written:

[3D] case $\dfrac{\frac{H}{D}}{\frac{L_s}{D}} \approx \text{Tan}\,\theta$

θ is three dimensional separation shock angle which varies with Mach number

[2D] case $\dfrac{H}{L_s} = \text{Tan}\,[\delta_w]$

δ_w is the two-dimensional separation angle which does not vary with Mach number

Lowson (Reference 17) showed that, for two-dimensional protuberances, the separated shear layer attaches near the top of a step and that the line joining the separation and reattachment points lies at an angle to the surface between 12 degrees and 15 degrees. A plot of the height compared to separation length shows that the line of correlation is an angle of 14.4 degrees (see Figure 38). The photograph given in Figure 39 shows that the separated shear layer passes over the top of the step and the dotted line indicates an approximate separation angle.

Zukoski (Reference 18) performed a literature survey of turbulent boundary layer separation in front of forward-facing steps and concluded that the separation angle was an average of 13 degrees. His data covered the range from Mach 1.4 to 5.0. Therefore for two-dimensional protuberances, the height to separation length ratio is a function of the separation angle which may vary from 12 to 15 degrees in the

Mach number range of 1.4 to 5.0. For three-dimensional, protuberances the normalized height to separation length is a function of the separation shock angle which varies from approximately 90 degrees at Mach 1 to 22 degrees at Mach 5.0.

5.0 CONCLUSIONS

Shadowgraph, pressure and flow visualization experiments have been performed on a series of cylindrical protuberances and two scale model Saturn V protuberances in the Marshall Space Flight Center's 14 by 14 inch transonic wind tunnel. These experiments supported the broad features of supersonic separated flow put forth in Reference 2. In detail it is concluded that:

(1) The data at M = 1.15 is suspect due to characteristic standing shock waves on the splitter plate.

(2) The boundary layer thickness at the center position were:

Mach	δ inches
.80	0.90
.90	0.98
1.15	0.28 - 0.40
1.96	0.10

There was a 12 percent variation in boundary layer thickness for the forward and aft positions at the splitter plate.

(3) The supersonic flow about the cylindrical protuberances was shown to be three-dimensional, and an empirical equation was derived which could be utilized in the prediction of separation upstream of protuberances.

$$\frac{L_s}{D} = \frac{\frac{H}{D} + .071\,\frac{1.14}{M^2 - 1} + \frac{.573}{(M^2 - 1)^2}}{\text{Tan}\ \theta}$$

where θ is the conical separation shock angle.

(4) At low Mach numbers, the bow shock standoff distance was considered a factor of dominating importance. It was predicted that the lambda shock system created by the intersection of the separation would coalesce to form one nearly normal shock as the Mach 1 was approached. Also, it was observed that the large standoff distances for the bow shock at low Mach numbers could influence the separation shock angle.

(5) The region of the wakes immediately behind the cylindrical protuberances which extended downstream for approximately one diameter was found to be a low pressure region. At Mach number 1.96, the necking down of the wake appeared to vary with height.

(6) The extent of the low pressure region of the cylindrical wake at transonic Mach numbers varied with height.

(7) The upstream separated flow in the transonic region was a function of height and diameter alone. The data at both Mach .8 and .9 were correlated by:

$$\frac{L_s}{D} = \frac{\frac{H}{D} + .38}{.53}$$

(8) For transonic flow, the separation length did not approach a constant as the ratio exceeded 1.0 because of the thickened boundary layer. The largest height to boundary layer thickness ratio was 2.0.

(9) Supersonic separation upstream of three-dimensional protuberances is proportional to the separation shock angle because this shock is allowed to approach the cylinder and enfold it, so that:

$$\frac{\frac{H}{D}}{\frac{L_s}{D}} \approx \text{Tan } \theta$$

whereas for two-dimensional protuberances, the separated shear layer must pass over the protuberance and because there is no side relief, the separation angle determined the separation length, so that:

$$\frac{H}{L_s} = \text{Tan } \delta_w$$

where δ_w = separation angle generally a constant ranging from 12 to 15 degrees for a particular set of flow conditions.

(10) The increase in the acoustic environment occurred near the protuberances and in some cases exceeded 6 dB at transonic speeds and 12 dB at supersonic speeds.

(11) At transonic speeds, the acoustic environment in the wake of the protuberance remained at a high level. This region of high acoustic environment extended two diameters back of the protuberance and the increase in the acoustic environment was 6 dB or more in certain cases.

REFERENCES

1. Reich, J.R., "Saturn V. External Protuberances, Cavities and Corrugations," Lockheed Missiles and Space Company, Huntsville Technical Memorandum, TM 54/50-43, May 1963.

2. Dendrinos Jr., Steve, "Prediction of Mean Flow Characteristics About Three-Dimensional Protuberances in Supersonic Flow," Wyle Laboratories Research Staff Report WR-67-19, November 1967.

3. Dendrinos Jr., Steve, "Test Program for the Investigation of Transonic and Supersonic Flows Around Protuberances," Wyle Laboratories Research Staff Technical Memorandum 67-7, October 1967.

4. Simon, Erwin, "Calibration Tests of the Marshall Space Flight Center 14- by 14-Inch Trisonic Wind Tunnel, NASA-TMX-53113, August 20, 1964.

5. Ames Research Staff, "Equations, Tables and Charts for Compressible Flow," NACA Report 1135, 1953.

6. Sykes, D.M., "The Supersonic and Low-Speed Flows Past Circular Cylinders of Finite Length Supported at One End," Journal of Fluid Mechanics, Vol. 12, Part 3, March 1962.

7. Lucero, E.F., "Turbulent Boundary Layer Separation Induced by Three-Dimensional Protuberances on a Flat Plate," Master Thesis, University of Maryland, 1966.

8. Walthrup, P. J., et al., "Flow Field in the Vicinity of Circular Protuberances on a Flat Plate in Supersonic Flow," Journal of Spacecraft and Rockets, Vol. 5, No. 1, pp. 127-128.

9. Voitenko, D.M., et al., "Supersonic Gas Flow Past a Cylindrical Protuberance on a Plate," Translation by John Hopkins University (AD 650 960) January 1967.

10. Halprin, R. W., "Study of the Separated Regions Caused by Two-Dimensional and Cylindrical Steps Mounted on a Flat Plate in a Supersonic Turbulent Flow," Master's Thesis, University of California, Los Angeles, 1964.

11. Uselton, J.C., "Fin Shock/Boundary-Layer Interaction Tests on a Flat Plate with Blunted Fins at M_D=3 and 5," Arnold Engineering Development Center Test Report 67-113, June 1967 (AD 815 760).

12. Price Jr., E.A., and Stalling Jr., R.L., "Investigation of Turbulent Separated Flows in the Vicinity of Fin-Type Protuberances at Supersonic Mach Numbers," NASA TN D-3804, February 1967.

13. Miller, W.H., "Pressure Distributions on Single and Tandem Cylinders Mounted on a Flat Plate in Mach Number 510 Flow," University of Texas, Defense Research Laboratory Report 538, (N66-28598), June 1966.

14. Westkemper, J.C., "The Drag of Cylinders All or Partially Immersed in a Turbulent Supersonic Boundary Layer," University of Texas, Defense Research Laboratory Report 549, (AD 813 886) March 1967.

15. Amick, J.L., "Pressure Measurements on Sharp and Blunt 5° and 15° Half-Angle Cones at Mach Numbers 3.86 and Angles of Attack up to 100°," NASA TN D-753, February 1961.

16. Goldstein, S., "Modern Developments in Fluid Dynamics," Volumes I and II, Dover Publications, New York.

17. Lowson, M.V., "Flow Visualization Experiments with Separated Supersonic Turbulent Flow," Wyle Laboratories Report WR 66-23, April 1966.

18. Zukoski, E.E., "Turbulent Boundary Layer Separation in Front of a Forward-Facing Step," AIAA Journal, Volume 5, No. 10, pp. 1746 - 1753, October 1967.

19. Chapman, D.R., Kuehn, D.M., and Larson, H.K., "Investigation of Separated Flows in Supersonic and Subsonic Streams with Emphasis on the Effect of Transition," NACA Report 1356, 1956.

ACKNOWLEDGEMENTS

The experimental program was executed by the Staff of the Marshall Space Flight Center wind tunnel under the direction of E. Simon and D. Cope of the Marshall Space Flight Center and S. Mallard and J. Magnum of Northrop Space Laboratories.

TABLE I

WIND TUNNEL TEST CONDITIONS

Run	Dia. In.	Ht. In.	Pos.	M	P_o	T^o	Q	R/L x 10^{-6}/Ft	Type Test	Comment
1	-	-	-	.80	7.0	100	6.3	5.8	SG+P	Clean Plate
2	.25	.5	C	↓	↓	↓	↓	↓	↓	
3	.50	1.0	C							
4	1.0	1.0	C							
5	1.0	1.0	F							
6	1.0	1.0	A							
7	RCS	RCS	C							
8	APU	APU	C							
9	-	-	-	.90	7.0	100	7.2	6.1	SG+P	Clean Plate
10	25	.50	C	↓	↓	↓	↓	↓	↓	
11	.50	1.0	C							
12	1.0	1.0	C							
13	1.0	1.0	F							
14	1.0	1.0	A							
15	RCS	RCS	C							
16	APU	APU	C							
17	-	-	-	1.15	7.0	100	8.8	6.5	SG+P	Clean Plate
18	.25	.50	C	↓	↓	↓	↓	↓	↓	
19	.50	1.0	C							
20	1.0	1.0	C							
21	1.0	1.0	F							
22	1.0	1.0	A							
23	RCS	RCS	C							
24	APU	APU	C							
25	-	-	-	1.96	15.0	100	10.7	7.8	SG+P	Clean Plate
26	1.0	.25	C	↓	↓	↓	↓	7.7	↓	
27	1.0	.50	↓					7.6		
28	1.0	1.0						↓		
29	1.0	2.0								
30	2.0	.25								
31	2.0	.50								
32	2.0	1.0								
33	2.0	2.0								

C = Center
F = Forward
A = Aft

SG = Shadowgraph
P = Pressure
O = Oil Flow

TABLE I (Continued)

Run	Dia. In.	Ht. In.	Pos.	M	P_o	T^o	Q	R/L x 10^{-6}/Ft	Type Test	Comment
34	RCS	RCS	C	1.96	15.0	100	10.8	7.6	SG+P	
35	APU	APU	C	↓	↓	↓	↓	↓	↓	
36-2	APU	APU	A							
37	-	-	-	1.96	15.0	100	10.8	7.2	P	Clean Plate
38	1.0	.25	C					7.6		
39	↓	.50	↓					↓		
40		1.0								
41		2.0								
42	2.0	.25	C		15.0	100	10.8	7.6		
43	↓	.50	↓		↓	↓	↓	↓		
44		1.0						7.4		
45		2.0						7.1		
46	RCS	RCS	↓		15.0	100	10.8	7.6		
47	APU	APU			↓	↓	↓	7.1		
48	APU	APU	A					7.2		
49	-	-	-	.80	7.0	100	6.3	5.5	P	Clean Plate
50	.25	.0625	C		↓	↓	↓	5.9	↓	
51	↓	.125	↓					↓		
52		.250								
53		.50								
54	.50	.125	C		7.0	100	6.3	5.9	P	
55	↓	.250	↓		↓	↓	↓	↓	↓	
56		.50								
57		1.0								
58	1.0	.25	C		7.0	100	6.3	5.9	P	
59	↓	.50	↓		↓	↓	↓	↓	↓	
60		1.0								
61		2.0								
62	1.0	.25	F		7.0	100	6.3	5.7	P	
63	↓	.50	↓		↓	↓	↓	↓	↓	
64		1.0								
65		2.0								

TABLE I (Continued)

Run	Dia. In.	Ht. In.	Pos.	M	P_o	T^o	Q	R/L x 10^{-6}/Ft	Type Test	Comment
66	1.0	.25	A	.80	7.0	100	6.3	5.7	P	
67	↓	.50	↓	↓	↓	↓	↓	↓	↓	
68		1.0								
69		2.0								
70	RCS	RCS	C		7.0	100	6.3	5.9		
71	APU	APU	C		↓	↓	↓	5.9		
72	APU	APU	A	↓				5.7	↓	
73	-	-	-	.90	7.0	100	7.2	5.9	P	Clean Plate
74	.25	.0625	C	↓	7.0	100	7.2	6.3	↓	
75	↓	.125	↓		↓	↓	↓	↓		
76		.50								
78-2	.50	.125	↓	↓	7.0	100	7.2	6.4	↓	
79	↓	.250			↓	↓	↓	↓		
80		.50								
81		1.0								
82	1.0	.25	↓	↓	7.0	100	7.2	6.5	↓	
83	↓	.50			↓	↓	↓	6.5		
84		1.0						6.4		
85		2.0						6.4		
86	1.0	.25	F	↓	7.0	100	7.2	6.0	↓	
87	↓	.50	↓		↓	↓	↓	↓		
88		1.0								
89		2.0								
90	1.0	.25	A	↓	7.0	100	7.2	6.0	↓	
91	↓	.50	↓		↓	↓	↓	↓		
92		1.0								
93		2.0								
94	RCS	RCS	C	↓	7.0	100	7.2	6.2	↓	
95	APU	APU	C		↓	↓	↓	6.3		
96	APU	APU	A					6.0		

TABLE I (Continued)

Run	Dia. In.	Ht. In.	Pos.	M	P_o	T^o	Q	$R_y/L \times 10^{-6}$/Ft	Type Test	Comment
97	-	-		1.15	7.0	100	8.7	6.2	P	Clean Plate
98	.25	.0625	C		7.0	100	8.7	6.3	P	
99		.125								
100		.250								
101		.50								
102-3	.50	.125	C		7.0	100	8.7	6.3		
103-3		.250								
104		.50								
105		1.0								
106	1.0	.25	C		7.0	100	8.7	6.4		
107		.50								
108		1.0								
109		2.0								
110	1.0	.25	F		7.0	100	8.7	6.4		
111		.50								
112		1.0								
113		2.0								
114	1.0	.25	A		7.0	100	8.7	6.4		
115		.50						6.2		
116		1.0						6.2		
117		2.0						6.2		
118	RCS	RCS	C		7.0	100	8.7	6.3		
119	APU	APU	C							
120	APU	APU	A							
121	.25	.50	C	1.15	7.0	100	8.7	6.3	0	
122	.50	1.0								
123	1.0	1.0								
124	RCS	RCS								
125	APU	APU								

TABLE I (Continued)

Run	Dia. In.	Ht. In.	Pos.	M	P_o	T^o	Q	R/L x 10^{-6}/Ft	Type Test	Comment
126	.25	.50	C	.90	7.0	100	7.2	6.3	0	
127	.50	1.0	↓	↓	↓	↓	↓	↓	↓	
128	1.0	1.0								
129	RCS	RCS								
130	APU	APU								
131	.25	.50	C	.80	7.0	100	6.3	5.9	0	
132	.50	1.0	↓	↓	↓	↓	↓	↓	↓	
133	1.0	1.0								
134	RCS	RCS								
135	APU	APU								
136	.25	.50	C	1.96	15.0	100	10.8	7.2	0	
137	.50	1.0	↓	↓	↓	↓	↓	↓	↓	
138	1.0	1.0								
139	1.0	2.0								
140	2.0	1.0								
141	—	—	—	.80	7.0	100	6.3	5.9	SG+P	Clean Plate
142	—	—	—	.90	↓	↓	7.2	6.3	↓	No Grit
143	—	—	—	1.15			8.8	6.5		
161	Boundary Layer Rake Data α = 0		—	.80	7.0	100	6.3	5.9	P	No Grit
162-1			—	.90	↓	↓	7.2	6.3	↓	
163			—	.80			6.3	5.9		
164			—	.90			7.2	6 3		Grit
169			—	1.15			8.8	6.5		
165	Boundary Layer Rake Data $\alpha = -2.5^o$		—	.80	7.0	100	6.3	5.9	P	Grit
166			—	.90	↓	↓	7.2	6.3	↓	
167			—	.80			6..	5.9		
168			—	.90			7.2	6.3		No Grit

TABLE II

PROTUBERANCE CONFIGURATION

Configuration	Diameter	Height	$\frac{H}{D}$
1	.25	.0625	.250
2	↓	.1250	.500
3	↓	.2500	1.000
4	↓	.5000	2.000
5	.50	.1250	.250
6	↓	.2500	.250
7	↓	.5000	1.000
8	↓	1.0000	2.000
9	1.0	.2500	.250
10	↓	.5000	.500
11	↓	1.0000	1.000
12	↓	2.0000	2.000
13	1.0	.2500	.250
14	↓	.5000	.500
15	↓	1.0000	1.000
16	↓	2.0000	2.000
17	1.0	.2500	.250
18	↓	.5000	.500
19	↓	1.0000	1.000
20	↓	2.0000	2.000
21	2.0	.2500	.125
22	↓	.5000	.250
23	↓	1.0000	.500
24	↓	2.0000	1.000
25	Model Reaction Control System (RCS) Motors		
26	Model Auxiliary Propulsion Unit System (APU)		
27	Clean Model with Grit		
270	Clean Model - No Grit		

TABLE III

SUMMARY OF CURRENT DATA OBTAINED AT MACH 1.96

H	D	$\frac{H}{D}$	Shadowgraph L_s/D	Pressure L_s/D	Oil L_s/D	Shadowgraph θ mean
.25	1.0	.25	.77	.75 - 1.0	1.0	40°
.50	↓	.50	1.20	1.0 - 1.25	1.1	39°
1.0	↓	1.0	1.59	1.5 - 2.0	1.5	40°
2.0	↓	2.0	1.99	1.75 - 2.25	2.0	42°
.25	2.0	.125	.52	-	-	38°
.50	↓	.250	.78	.75 - 1.0	-	41°
1.0	↓	.50	1.15	1.0 - 1.25	-	40°
2.0	↓	1.0	1.44	1.5 - 2.0	-	40°

Average θ = 40°

TABLE IV

MEASURED ACOUSTIC ENVIRONMENT - OVERALL SOUND PRESSURE LEVEL IN DECIBELS

M = .80

Run	D	H	Pos.	M1*	M2*	M3	M4	M5	M6	M7
49	-	-	-	161.5	158.5	158.0	158.5	160.0	158.5	157.5
50	.25	.0625	C	160.5	158.5	157.0	158.0	159.0	157.5	157.5
51	↓	.1250	↓	160.5	158.5	157.0	158.0	159.5	157.5	157.5
52	↓	.2500	↓	159.5	158.0	157.0	158.0	161.0	157.5	157.5
53	↓	.5000	↓	161.0	158.0	158.0	158.5	162.5	158.0	157.5
54	.50	.1250	↓	161.5	159.0	157.5	159.0	160.0	158.0	158.0
55	↓	.2500	↓	161.0	159.0	157.5	158.0	161.5	158.0	158.0
56	↓	.5000	↓	161.5	159.0	158.5	158.0	164.0	160.0	158.0
57	↓	1.000	↓	162.0	160.0	160.5	169.5	168.0	161.5	160.0
58	1.0	.2500	↓	161.5	159.5	158.0	158.5	161.5	158.0	158.0
59	↓	.5000	↓	163.5	160.0	160.5	159.0	163.5	160.5	159.0
60	↓	1.000	↓	164.0	161.0	163.5	160.0	166.5	167.5	161.5
61	↓	2.000	↓	166.5	161.0	163.0	159.5	167.0	165.0	162.0
62	1.0	.2500	F	163.5	159.0	157.0	158.0	159.5	158.0	159.5
63	↓	.5000	↓	165.5	161.5	159.0	158.0	160.5	159.0	160.0
64	↓	1.000	↓	169.0	166.0	162.5	159.5	165.5	163.0	161.0
65	↓	2.000	↓	166.0	162.5	164.0	160.0	167.0	167.0	161.0
66	1.0	.2500	A	161.0	158.5	157.5	158.0	165.0	158.5	160.0
67	↓	.5000	↓	159.5	158.5	157.5	158.5	167.0	160.0	161.0
68	↓	1.000	↓	161.0	159.0	158.5	158.5	166.0	161.0	165.5
69	↓	2.000	↓	162.0	159.0	158.5	158.5	166.0	161.5	167.0
70	RCS	-	C	161.5	158.5	158.0	158.0	160.0	158.0	157.0
71	APU	-	C	160.0	159.0	157.5	158.5	156.0	157.0	158.5
72	APU	-	A	161.0	158.0	157.5	158.0	157.0	161.5	160.5

M = Microphone
C = Center
F = Forward
A = Aft

*To obtain correct values for Microphone 1 and 2 add .58 and 1.13 dB respectively.

TABLE IV (Continued)

M = .90

Run	D	H	Pos.	M1*	M2*	M3	M4	M5	M6	M7
73	-	-	-	161.0	159.5	159.0	160.0	160.0	159.5	159.0
74	.25	.062	C	160.5	158.5	158.0	160.0	160.0	158.0	158.0
75	↓	.125	↓	160.5	158.5	158.5	159.5	160.0	158.0	157.5
76	↓	.250	↓	160.5	158.5	158.5	160.0	162.0	158.5	158.5
77	↓	.500	↓	161.0	159.0	159.5	160.0	163.5	159.0	158.0
78	.50	.125	↓	160.0	158.5	158.5	159.5	160.5	158.0	158.0
79	↓	.250	↓	161.0	158.5	159.0	159.5	162.5	158.5	158.0
80	↓	.500	↓	162.0	159.0	159.5	160.0	165.5	160.5	158.5
81	↓	1.00	↓	162.0	159.5	160.0	160.0	169.5	164.0	160.0
82	1.0	.250	↓	162.0	159.0	159.5	159.5	162.0	158.5	158.0
83	↓	.500	↓	164.0	160.5	161.5	160.0	165.0	164.0	159.0
84	↓	1.00	↓	160.5	161.5	164.0	160.5	169.0	169.0	163.0
85	↓	2.00	↓	160.0	163.0	164.0	160.5	165.5	164.0	164.5
86	1.0	.250	F	163.5	160.0	159.0	160.0	160.5	158.5	158.5
87	↓	.500	↓	165.0	163.0	160.0	160.0	162.5	160.0	159.0
88	↓	1.00	↓	169.0	166.5	164.5	161.5	166.0	165.5	160.5
89	↓	2.00	↓	165.0	163.0	163.5	162.5	168.0	168.5	162.0
90	1.0	.250	A	160.5	159.5	158.5	160.0	166.0	160.5	158.5
91	↓	.500	↓	160.5	160.0	159.5	160.0	168.0	161.5	162.0
92	↓	1.00	↓	161.0	160.0	159.5	160.0	167.5	162.5	166.0
93	↓	1.00	↓	161.0	160.0	159.5	160.5	168.0	164.5	168.0
94	RCS	-	C	163.0	159.5	159.5	160.0	161.0	159.0	158.5
95	APU	-	C	161.5	160.0	159.0	160.0	158.0	159.0	159.5
96	APU	-	A	161.0	159.5	159.0	159.5	158.0	160.5	160.5

TABLE IV (Continued)

M = 1.15

Run	D	H	Pos.	M1*	M2*	M3	M4	M5	M6	M7
97	-	-	-	162.5	160.5	159.5	161.0	161.0	161.0	159.5
98	.25	.062	C	161.5	160.0	159.0	161.0	160.5	160.0	160.0
99	↓	.125	↓	162.0	160.0	159.5	161.5	161.0	160.5	160.0
100	↓	.250	↓	161.5	160.0	159.0	161.0	162.0	160.0	160.0
101	↓	.500	↓	161.5	160.0	159.0	161.0	162.0	160.5	159.5
102-3	.50	.125	↓	162.5	160.5	159.0	160.5	162.0	160.0	159.5
103-3	↓	.250	↓	162.0	160.5	159.0	160.5	170.0	160.5	160.0
104	↓	.500	↓	163.0	160.5	159.0	160.5	165.0	161.0	160.0
105	↓	1.00	↓	164.0	161.0	161.0	160.5	162.5	160.0	160.0
106	1.0	.250	↓	162.0	160.5	159.0	161.0	164.0	161.0	160.0
107	↓	.500	↓	170.0	162.5	163.5	170.0	163.0	160.5	160.5
108	↓	1.00	↓	169.0	168.5	162.5	163.5	161.5	160.0	161.0
109	↓	2.00	↓	167.5	166.5	162.0	164.0	160.5	159.0	164.0
110	1.0	.250	F	162.5	160.5	159.0	160.5	162.5	160.5	160.0
111	↓	.500	↓	161.5	160.0	160.5	160.5	165.0	161.0	160.0
112	↓	1.00	↓	162.0	160.5	50.5	161.5	166.0	165.0	160.0
113	↓	2.00	↓	161.5	160.5	159.5	160.5	166.5	165.0	161.5
114	1.0	.250	A	161.5	160.0	159.5	160.5	159.0	159.5	160.0
115	↓	.500	↓	162.0	160.0	159.0	160.5	168.5	165.0	164.0
116	↓	1.00	↓	163.0	160.5	160.0	160.5	168.0	167.5	164.5
117	↓	2.00	↓	162.5	160.5	161.0	161.0	167.0	166.0	165.5
118	RCS	-	C	162.5	160.5	158.5	160.5	163.0	160.5	159.5
119	APU	-	C	160.5	160.0	158.5	160.5	160.0	159.0	160.0
120	APU	-	A	160.0	160.0	159.0	160.5	157.5	159.5	160.5

TABLE IV (Continued)

M = 1.96

Run	D	H	Pos.	M1*	M2*	M3	M4	M5	M6	M7
37	-	-	-	162.5	161.0	160.0	161.0	162.0	160.0	160.0
38	1.0	.250	C	164.0	162.0	162.0	161.5	164.0	160.0	160.0
39	↓	.500	↓	167.5	164.5	162.5	162.0	162.5	160.0	159.5
40	↓	1.00	↓	169.0	166.0	164.5	165.0	162.0	160.0	161.0
41	↓	2.00	↓	170.0	167.5	169.0	166.0	163.0	160.0	161.0
42	2.0	.250	↓	169.5	164.0	160.0	162.0	161.0	161.0	159.5
43	↓	.500	↓	173.5	168.5	163.0	165.0	161.0	159.5	160.0
44	↓	1.00	↓	174.5	172.0	163.0	165.5	161.5	160.0	162.0
45	↓	2.00	↓	174.0	172.0	-	170.0	168.0	160.0	163.5
46	RCS	-	↓	163.0	160.5	160.0	161.5	162.0	160.0	159.5
47	APU	-	↓	162.0	162.0	159.5	162.0	161.5	159.5	161.5
48	APU	-	A	163.0	161.5	160.0	[illegible]	160.0	160.0	160.0

TABLE V

INCREASE IN ACOUSTIC ENVIRONMENT DUE TO PROTUBERANCES - PRESENTED AS DECIBELS WHERE $\Delta dB = OSPL_{PROTUBERANCE} - OSPL_{CLEAN\ PLATE}$

M = .80

Run	D	H	Pos.	M1	M2	M3	M4	M5	M6	M7
50	.25	.062	C	-1.0	0	-1.0	-0.5	-1.0	-1.0	0
51	↓	.125	↓	-1.0	0	-1.0	-0.5	-0.5	-1.0	0
52	↓	.250	↓	-2.0	-0.5	-1.0	-0.5	1.0	-1.0	0
53	↓	.500	↓	-0.5	-0.5	0	0	2.5	-0.5	0
54	.50	.125	↓	0	-0.5	-0.5	0.5	0	-0.5	0.5
55	↓	.250	↓	-0.5	0.5	-0.5	-0.5	1.5	-0.5	0.5
56	↓	.500	↓	0	0.5	0.5	-0.5	4.0	1.5	0.5
57	↓	1.00	↓	0.5	1.5	2.5	1.0	8.0	3.0	2.5
58	1.0	.250	↓	0	1.0	0	0	1.5	-0.5	0.5
59	↓	.500	↓	2.0	1.5	2.5	0.5	3.5	2.0	1.5
60	↓	1.00	↓	2.5	2.5	5.5	1.5	6.5	9.0	4.0
61	↓	2.00	↓	5.0	2.5	5.0	1.0	7.0	7.0	4.5
62	1.0	.250	F	2.0	0.5	-1.0	-0.5	-0.5	-0.5	2
63	↓	.500	↓	4.0	3.0	1.0	-0.5	0.5	0.5	2.5
64	↓	1.00	↓	7.5	7.5	4.5	1.0	5.5	5.0	3.5
65	↓	2.00	↓	4.5	4.0	6.0	1.5	7.0	9.0	3.5
66	1.0	.250	A	-0.5	0	-0.5	-0.5	5.0	0	2.5
67	↓	.500	↓	-2.0	0	-0.5	0	7.0	1.5	3.5
68	↓	1.00	↓	-0.5	0.5	0.5	0	6.0	2.5	8.0
69	↓	2.00	↓	0.5	0.5	0.5	0	6.0	3.0	10.0
70	RCS	-	C	0	0	0	-0.5	0	-0.5	-0.5
71	APU	-	C	-1.5	0.5	-0.5	0	-4.0	-1.5	1.0
72	APU	-	A	-0.5	-0.5	-0.5	-0.5	-0.3	3.0	3.0

M = Microphone
C = Center
F = Forward
A = Aft

TABLE V (Continued)

M = .90

Run	D	H	Pos.	M1	M2	M3	M4	M5	M6	M7
74	.25	.0625	C	-0.5	-1.0	-1.0	0	0	-1.5	-1.0
75	↓	.1250	↓	-0.5	-1.0	-0.5	-0.5	0	-1.5	-1.5
76	↓	.2500	↓	-0.5	-1.0	-0.5	0	2.0	-1.0	-1.0
77	↓	.5000	↓	0	-0.5	0.5	0	3.5	-0.5	-1.0
78	.50	.1250	↓	-1.0	-1.0	-0.5	-0.5	0.5	-1.5	-1.0
79	↓	.2500	↓	0	-1.0	0	-0.5	2.5	-1.0	-1.0
80	↓	.5000	↓	1.0	-0.5	0.5	0	5.5	1.0	-0.5
81	↓	1.000	↓	1.0	0	1.0	0	9.5	4.5	1.0
82	1.0	.2500	↓	1.0	-0.5	0.5	-0.5	2.0	-1.0	-1.0
83	↓	.5000	↓	3.0	1.0	2.5	0	5.0	4.5	0
84	↓	1.000	↓	-0.5	2.0	5.0	0.5	9.0	9.5	4.0
85	↓	2.000	↓	8.0	3.5	5.0	0.5	5.5	4.5	5.5
86	1.0	.2500	F	2.5	0.5	0	0	0.5	-1.0	-0.5
87	↓	.5000	↓	4.0	3.5	1.0	0	2.5	0.5	0
88	↓	1.000	↓	8.0	7.0	5.5	1.5	6.0	6.0	1.5
89	↓	2.000	↓	4.0	3.5	4.5	2.5	8.0	9.0	3.0
90	1.0	.2500	A	-0.5	0	-0.5	0	6.0	1.0	-0.5
91	↓	.5000	↓	-0.5	0.5	0.5	0	8.0	2.0	3.0
92	↓	1.000	↓	0	0.5	0.5	0	7.5	3.0	7.0
93	↓	2.000	↓	0	0.5	0.5	0.5	8.0	5.0	9.0
94	RCS	-	C	2.0	0	0.5	0	1.0	-0.5	-0.5
95	APU	-	C	0.5	0.5	0	0	-2.0	-0.5	0.5
96	APU	-	A	0	0	0	-0.5	-2.0	1.0	1.5

TABLE V (Continued)

M = 1.15

Run	D	H	Pos.	M1	M2	M3	M4	M5	M6	M7
98	.25	.062	C	-1.0	-0.5	-0.5	0	-0.5	-1.0	0.5
99	↓	.125	↓	-0.5	-0.5	0	0.5	0	-0.5	0.5
100		.250		-1.0	-0.5	-0.5	0	1	-1.0	0.5
101		.500		-1.0	-0.5	-0.5	0	1	-0.5	0
102	.50	.125		0	0	-0.5	-0.5	1.0	-1.0	0
103	↓	.250		-0.5	0	-0.5	-0.5	9.0	-0.5	0.5
104		.500		0.5	0	-0.5	-0.5	4.0	0	0.5
105		1.00		1.5	0.5	1.5	-0.5	1.5	-1.0	0.5
106	1.0	.250		-0.5	0	-0.5	0	3.0	0	0.5
107	↓	.500		7.5	2.0	4.0	9.0	2.0	-0.5	1.0
108		1.00		6.5	8.0	3.0	2.5	0.5	-1.0	1.5
109		2.00	↓	4.5	6.0	2.5	3.0	-0.5	-2.0	4.5
110	1.0	.250	F	0	0	-0.5	-0.5	1.5	-0.5	0.5
111	↓	.500	↓	-1.0	-0.5	1.0	-0.5	4.0	0	0.5
112		1.00		-0.5	0	1.0	0.5	5.0	4.0	0.5
113		2.00		-1.0	0	0	-0.5	5.5	4.0	2.0
114	1.0	.250	A	-1.0	-0.5	0	-0.5	-2.0	-1.5	0.5
115	↓	.500	↓	-0.5	-0.5	-0.5	-0.5	7.5	4.0	4.5
116		1.00		0.5	0	0.5	-0.5	7.0	6.5	5.0
117		2.00		0	0	1.5	0	6.0	5.0	6.0
118	RCS	-	C	0	0	-1.0	-0.5	2.0	-0.5	0
119	APU	-	C	-2.0	-0.5	-1.0	-0.5	-1.0	-2.0	0.5
120	APU	-	A	-2.5	-0.5	-0.5	-0.5	-3.5	-1.5	1.0

TABLE V (Continued)

M = 1.96

Run	D	H	Pos.	M1	M2	M3	M4	M5	M6	M7
38	1.0	.250	C	1.5	1.0	2.0	0.5	2.0	0	0
39	↓	.500	↓	5.0	3.5	2.5	1.0	0.5	0	-0.5
40	↓	1.00	↓	6.5	5.0	4.5	4.0	0	0	1.0
41	↓	2.00	↓	7.5	6.5	9.0	5.0	1.0	0	1.0
42	2.0	.250	↓	7.0	3.0	0	1.0	-1.0	1.0	-0.5
43	↓	.500	↓	11.0	7.5	3.0	4.0	-1.0	-0.5	0
44	↓	1.00	↓	12.0	11.0	3.0	4.5	-0.5	0	2.0
45	↓	2.00	↓	11.5	11.0	-	9.0	6.0	0	3.5
46	RCS	-	↓	0.5	-0.5	0	0.5	0	0	-0.5
47	APU	-	↓	-0.5	1.0	-0.5	1.0	-0.5	-0.5	1.5
48	APU	-	A	0.5	0.5	0	0	-2.0	0	0

1. 500 PSI Air Storage Tank
2. Control Valve
3. Settling Chamber and Heat Exchanger
4. Test Section
5. Diffuser
6. Auxiliary Vacuum Line
7. Atmospheric Exhaust Tower
8. Vacuum Field
9. Tunnel Control Console
10. Data Acquisition System
11. Multiple Pressure Scanning System

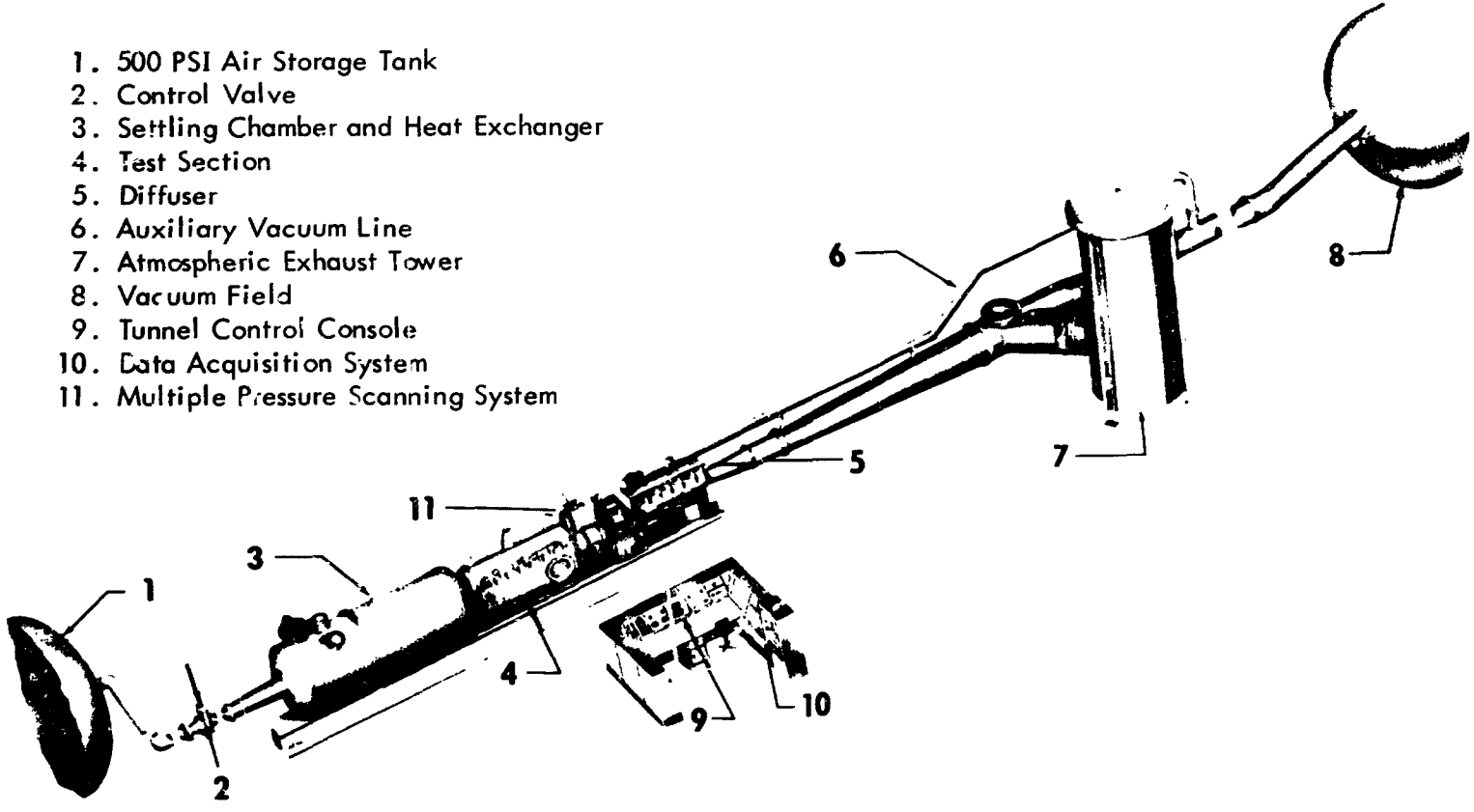

Figure 1. Photograph of the MSFC 14- by 14-Inch Trisonic Wind Tunnel

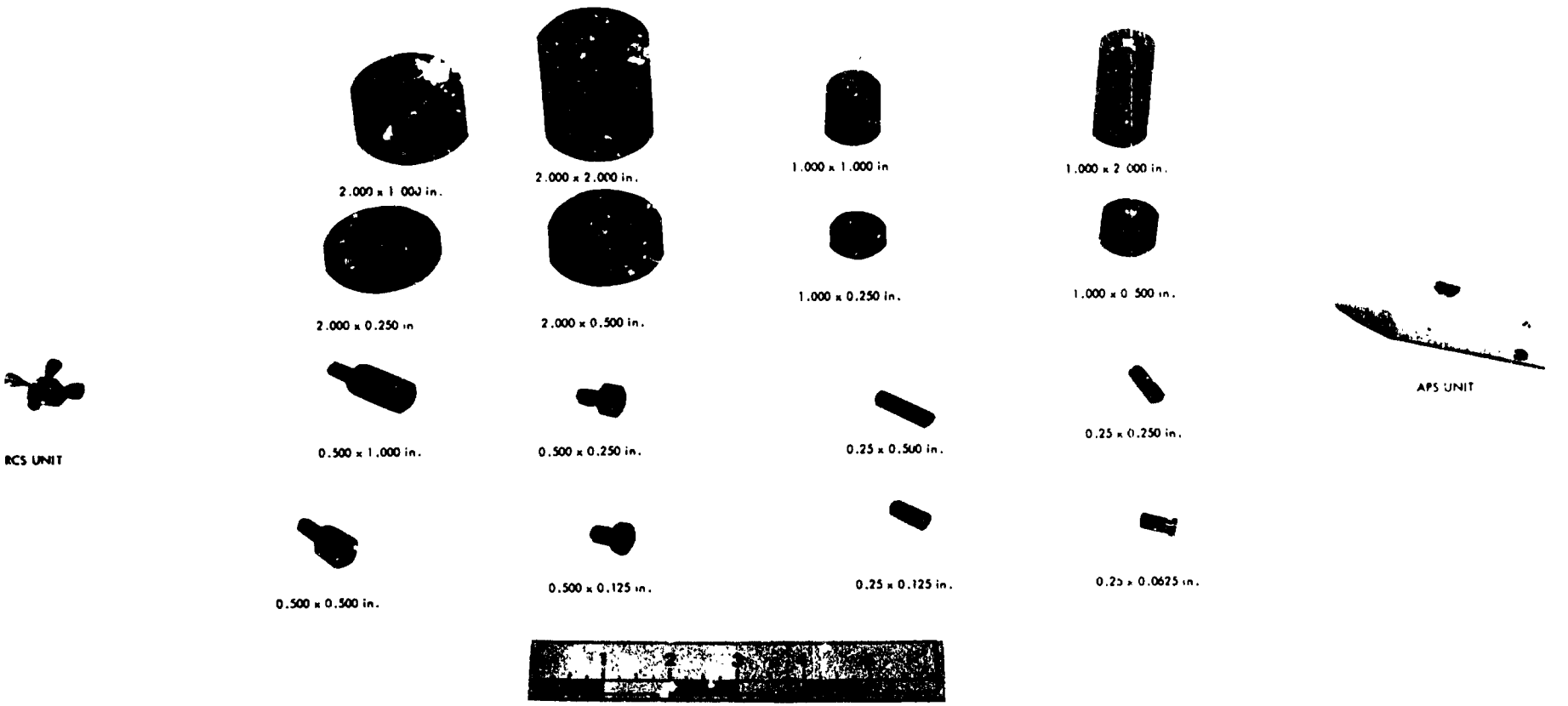

Figure 2. Photograph of Test Specimens

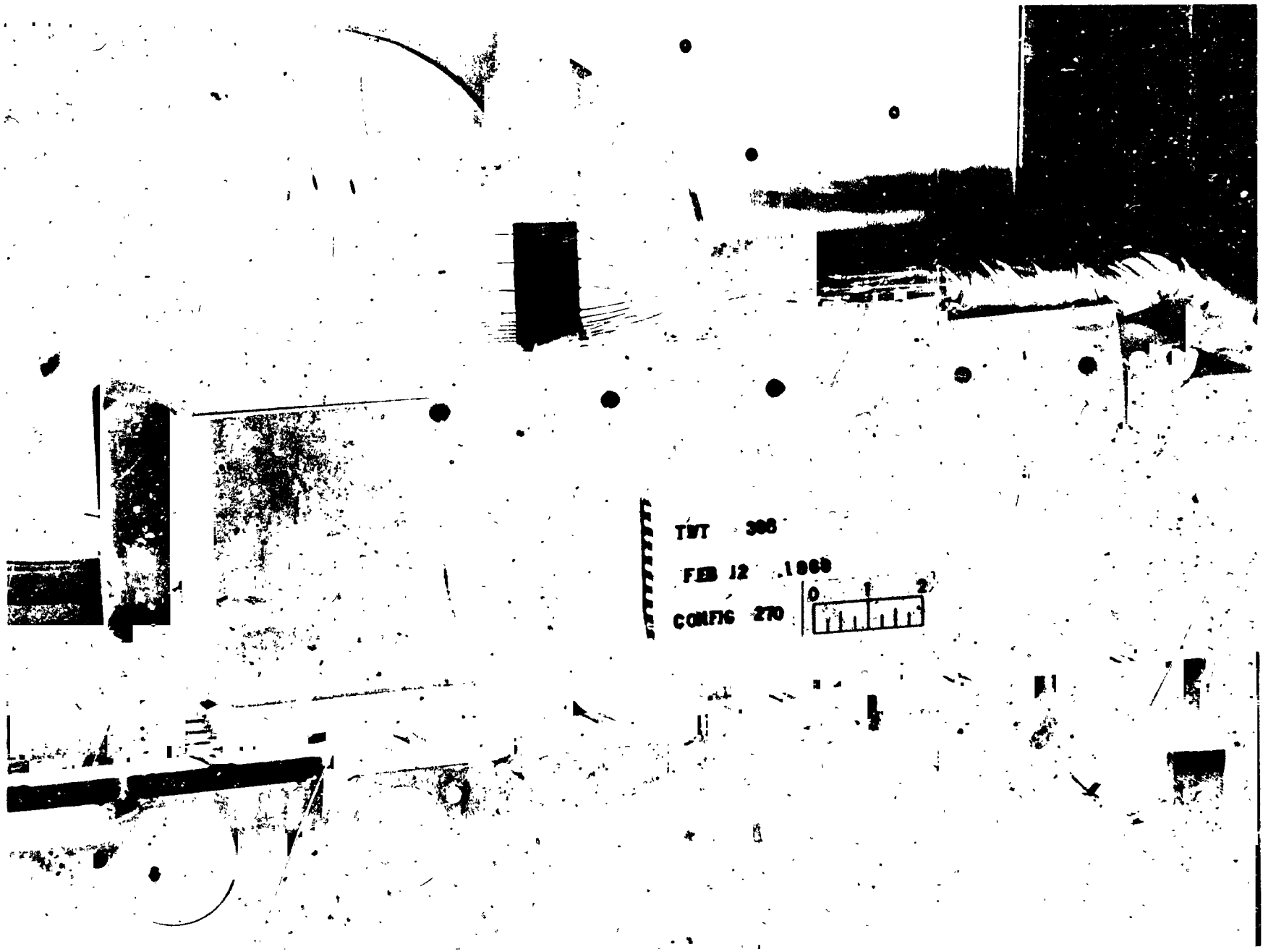

Figure 3. Photograph of Boundary Layer Rake Installed on the Splitter Plate, Which is Mounted in the Wind Tunnel

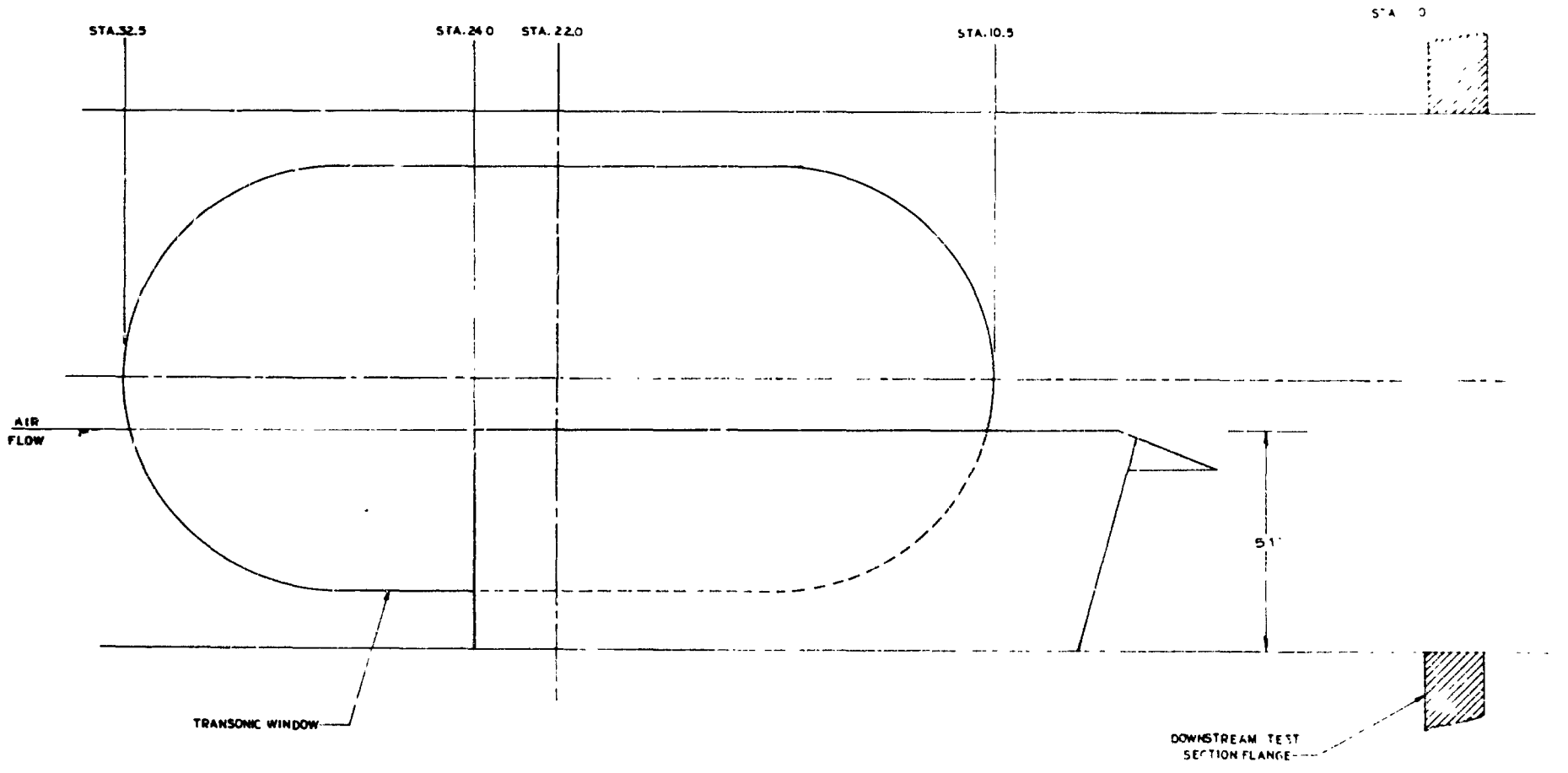

Figure 4. Splitter Plate Mounted in the MSFC 14- by 14-Inch Transonic Wind Tunnel.

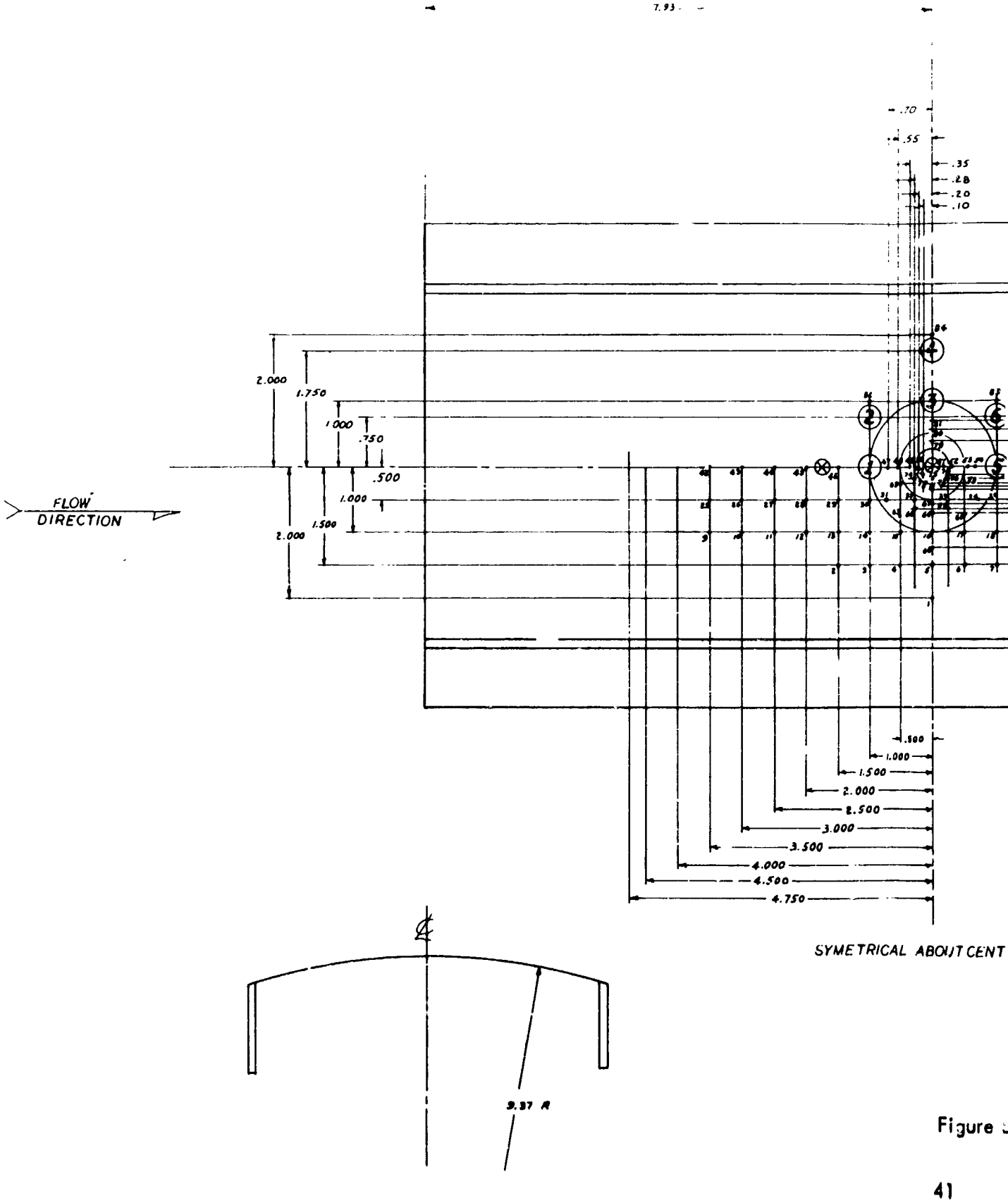

SECTION A-A

Figure

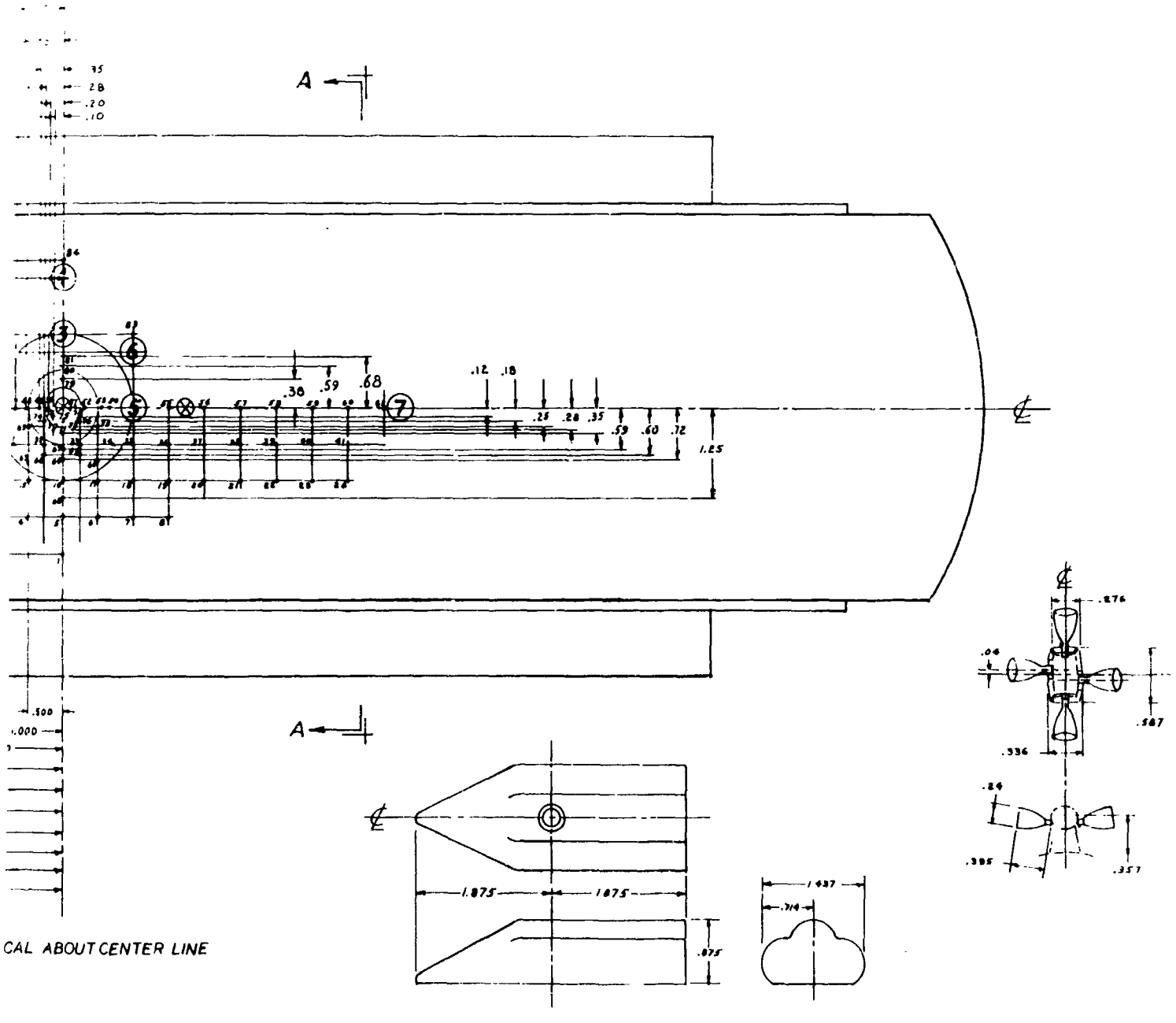

Figure 5. Measurement Locations for Model Splitter Plate.

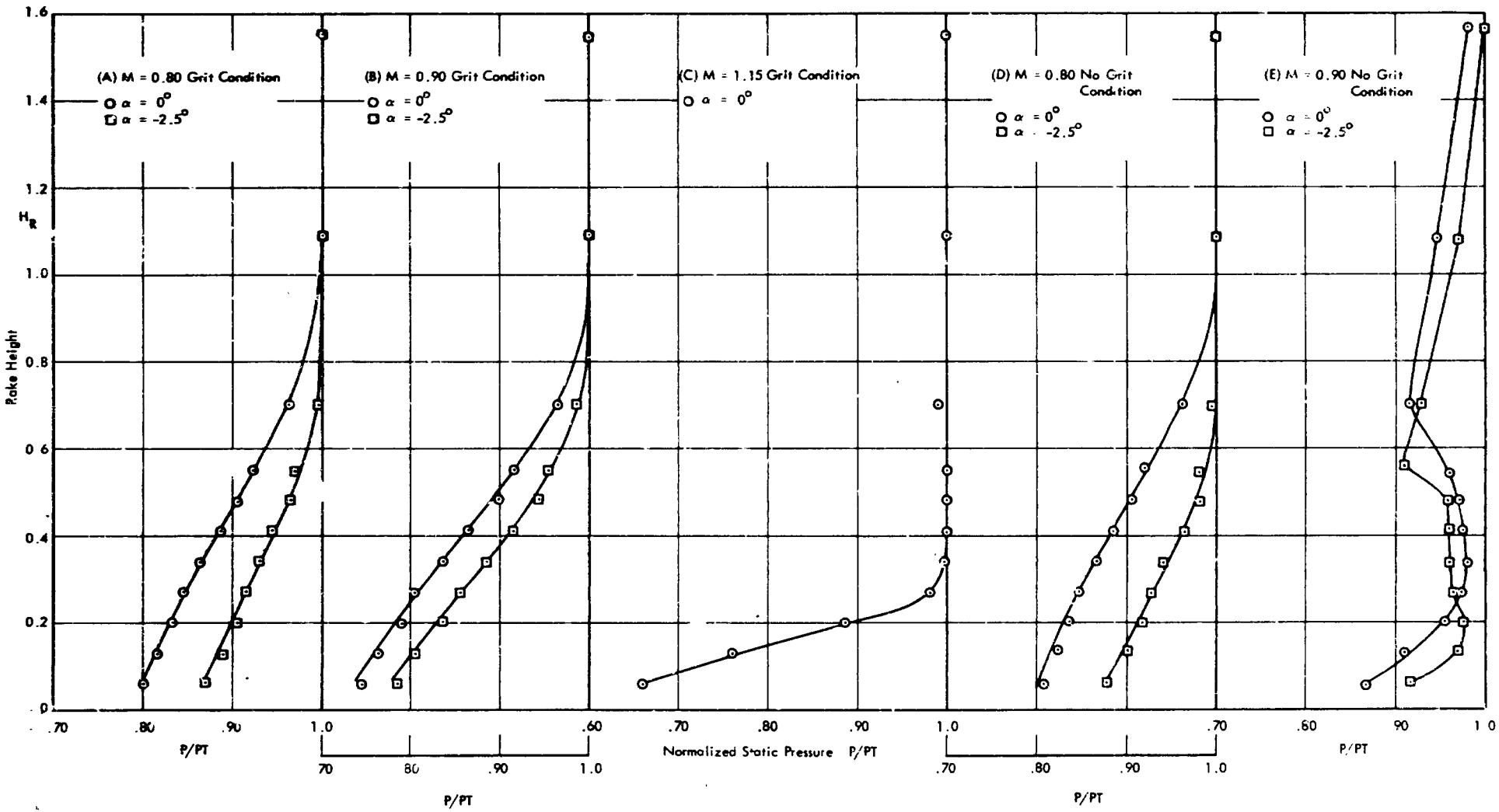

Figure 6. Pressure Profile from Boundary Layer Rake.

(a) $M_\infty = .80$

(b) $M_\infty = .90$

(c) $M_\infty = 1.15$

Figure 7. Shadowgraphs of Clean Plate with Grit Near the Leading Edge

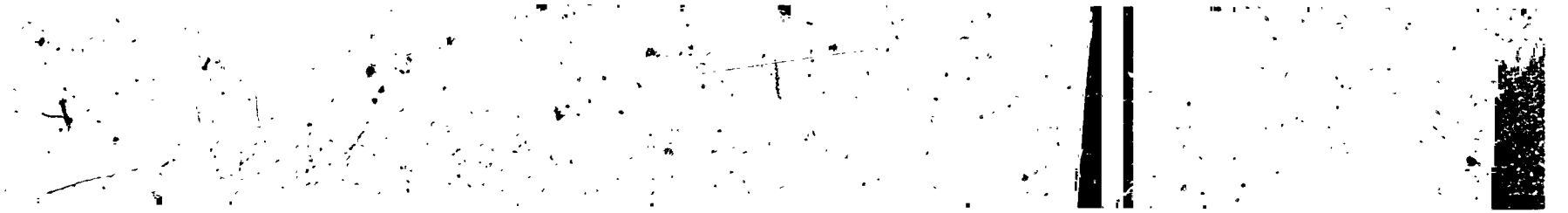

(a) M = .80

(b) M = .90

(c) M = 1.15

(d) M = 1.96

Figure 8. Shadowgraphs of Clean Plate Without Grit

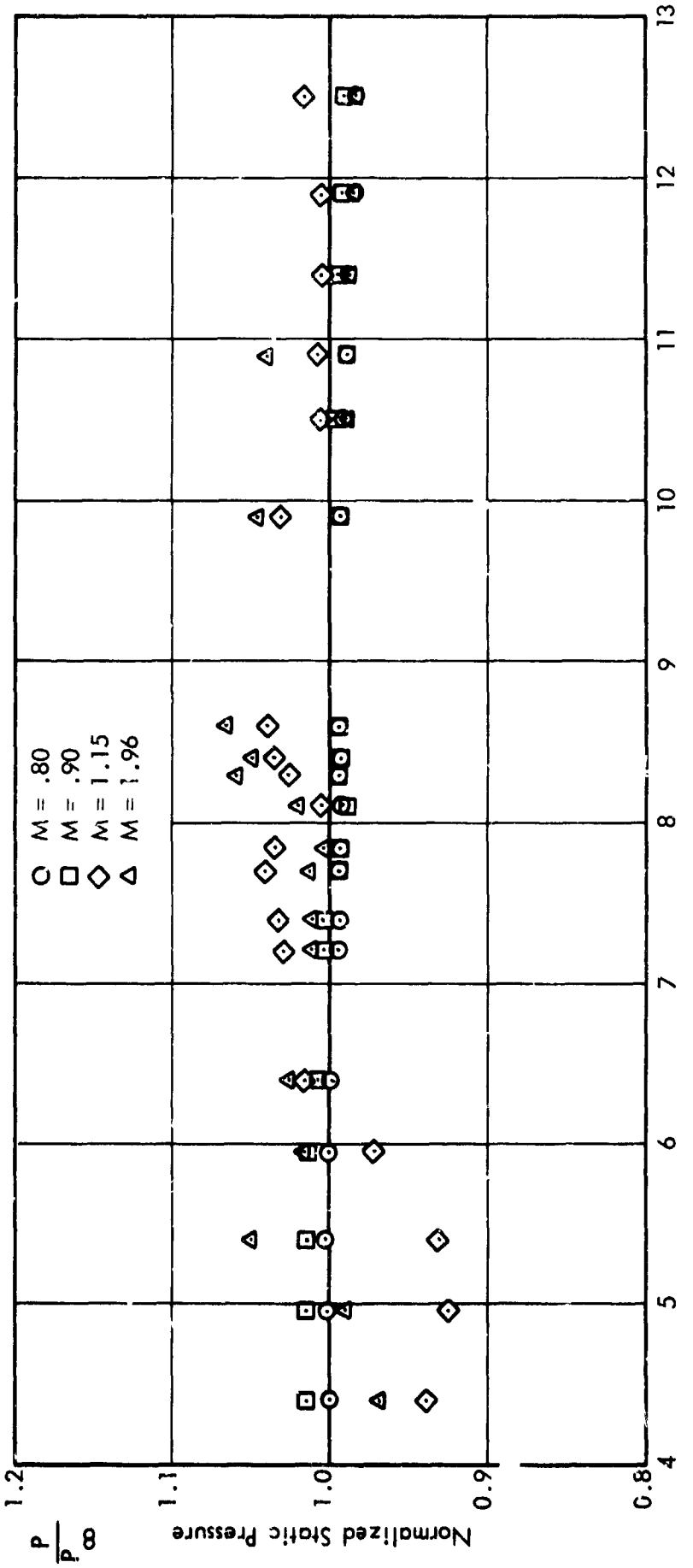

Figure 9. Pressure Profile Down the Centerline of the Splitter Plate - Clean Configuration

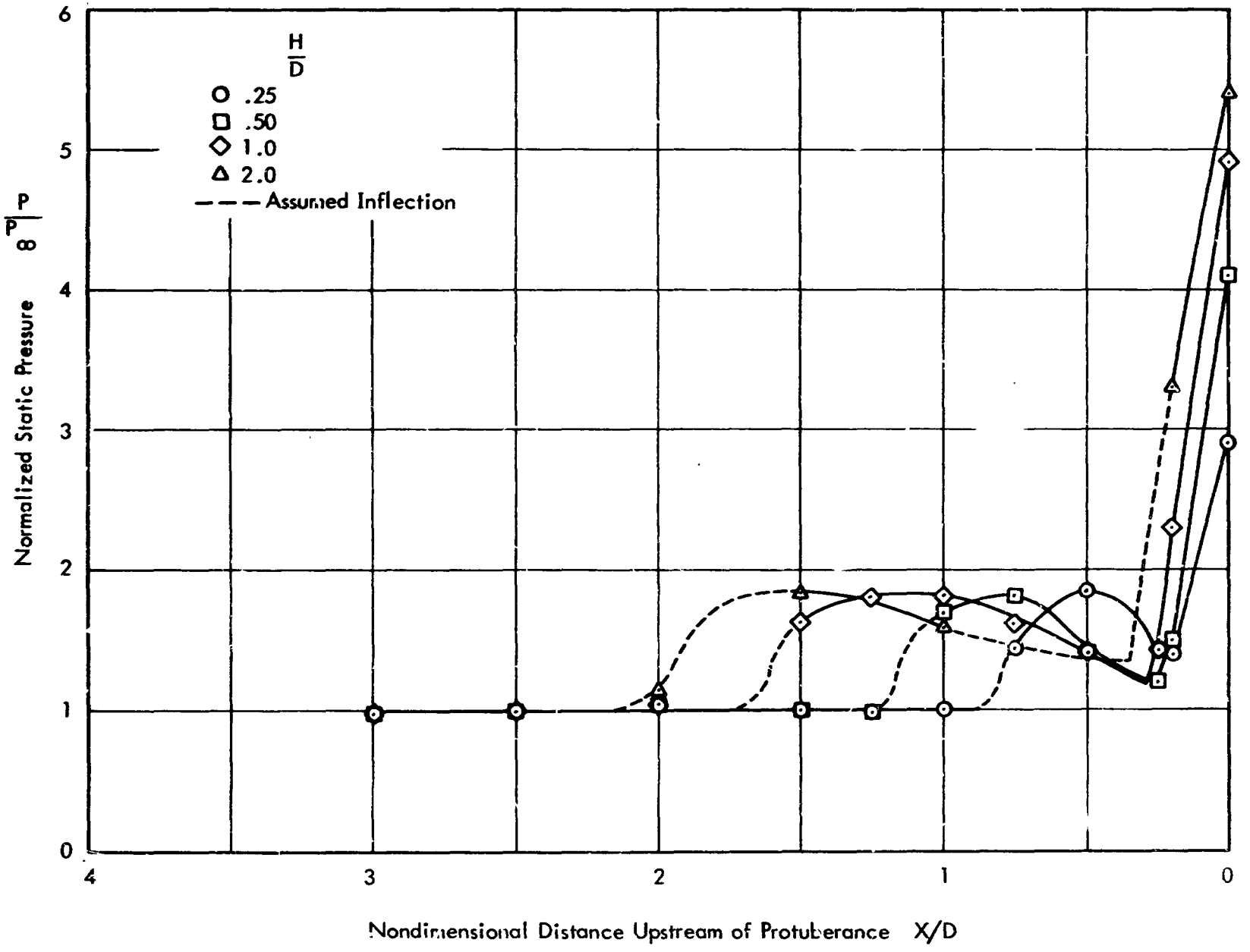

Figure 10. Upstream Centerline Pressure Profile for Cylindrical Protuberance at Mach 1.96

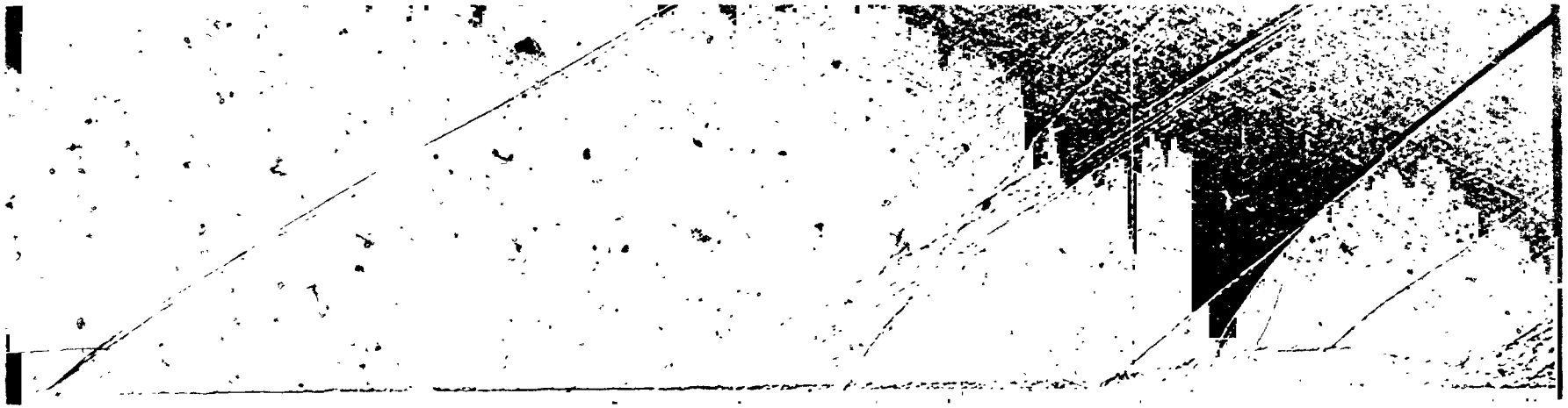

(a) H = .25

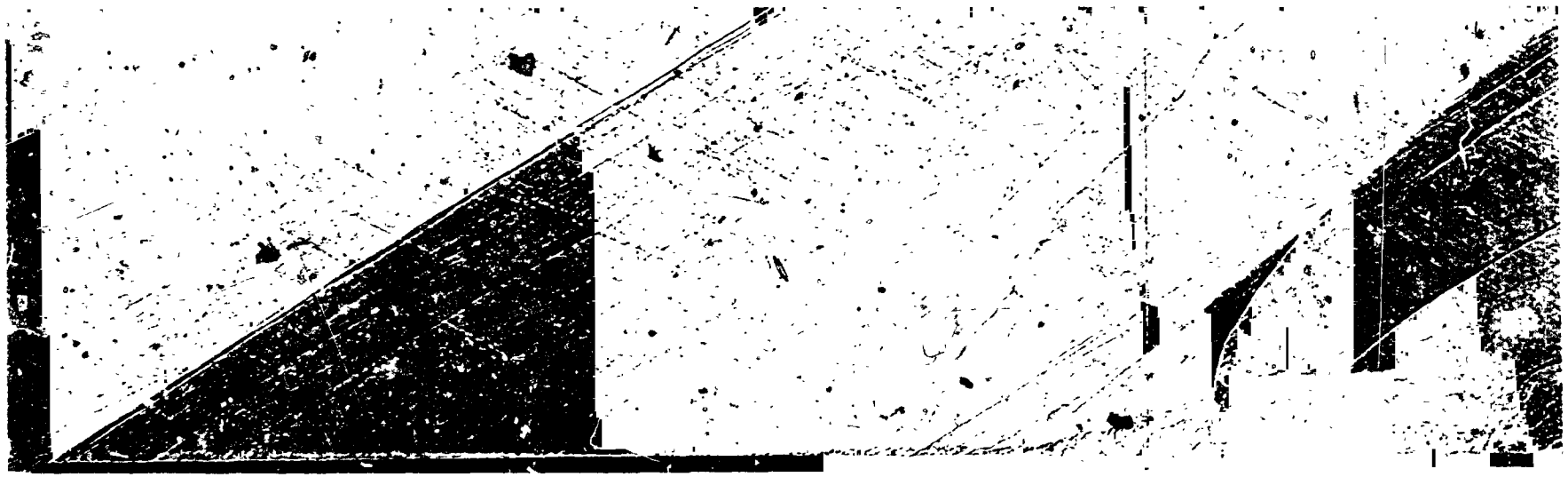

(b) H = .50

Figure 11. Shadowgraphs of 1-Inch Cylinder at Mach 1.96

Figure 12. Shadowgraph of 1-Inch Cylinder at Mach 1.96 and Height = 1.0 Inch

Figure 13. Shadowgraph of 1-Inch Cylinder at Mach 1.96 and Height = 2.0 Inches

(a) H = .25 Inch

(b) H = .50 Inch

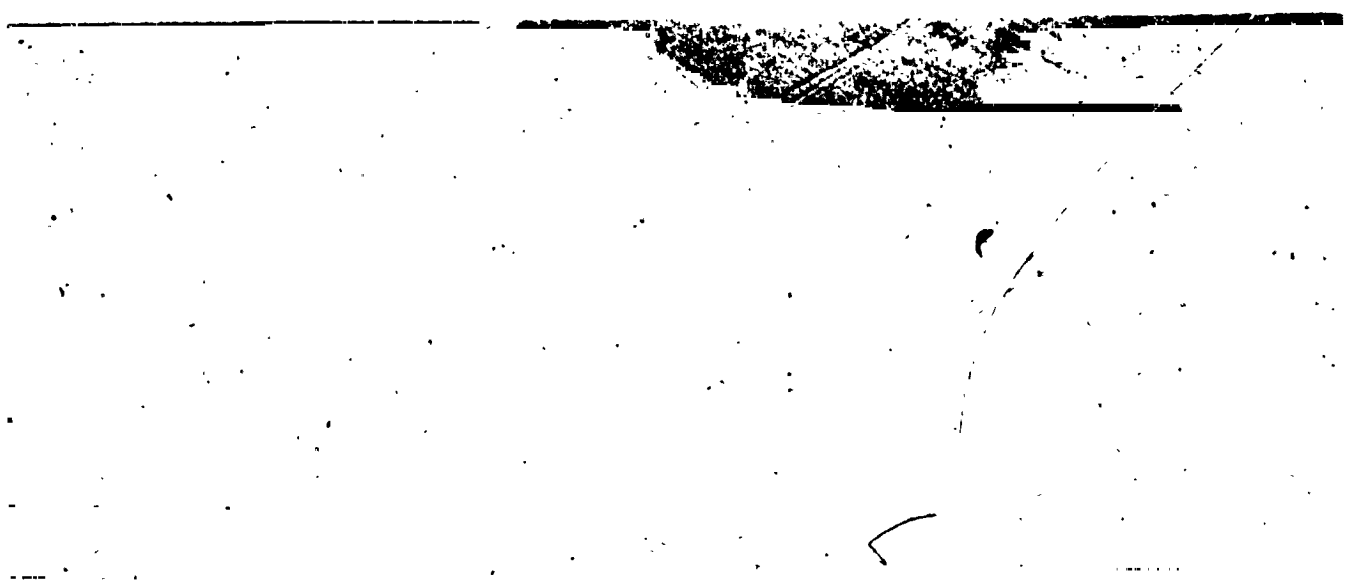

(c) H = 1.0 Inch

Figure 14. Shadowgraph of 2-inch Cylinder at Mach 1.96

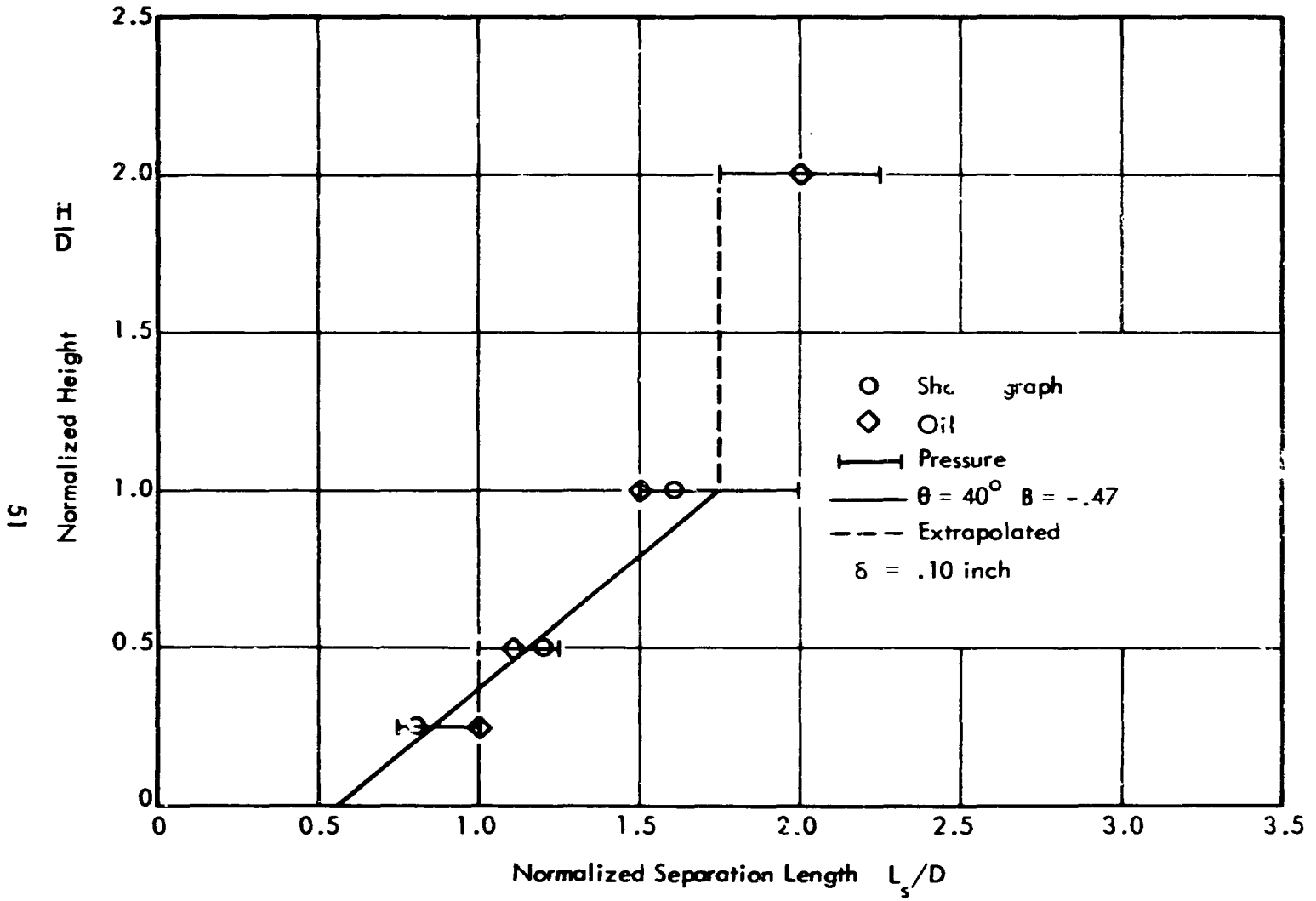

Figure 15. Correlation of Normalized Height with Normalized Separation Length for Cylindrical Protuberances at Mach 1.96

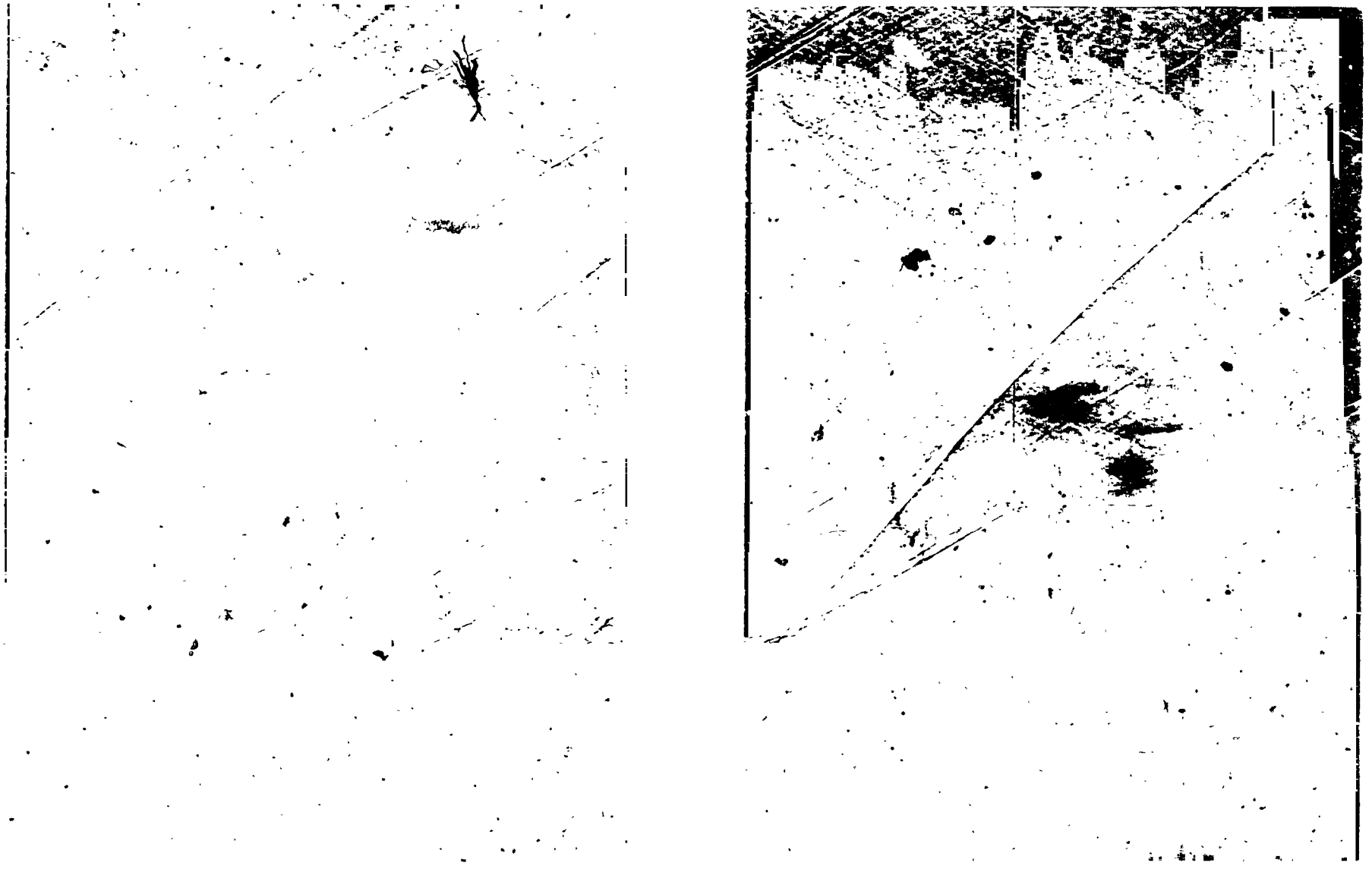

(a) RCS Motors

(b) APU

Figure 16. Shadowgraphs of the Saturn V Model Protuberances at Mach 1.96

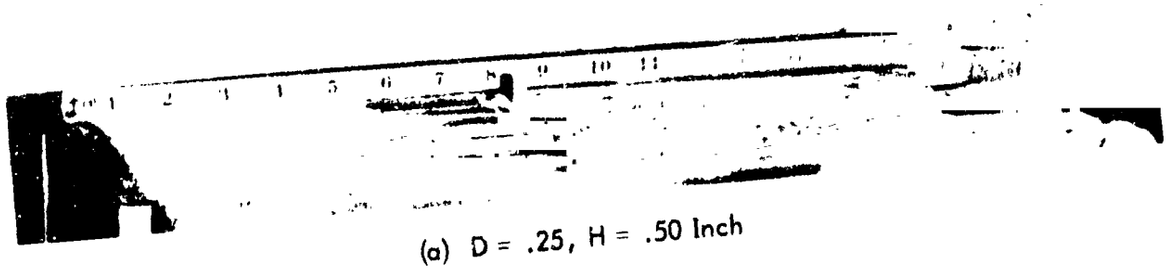

(a) D = .25, H = .50 Inch

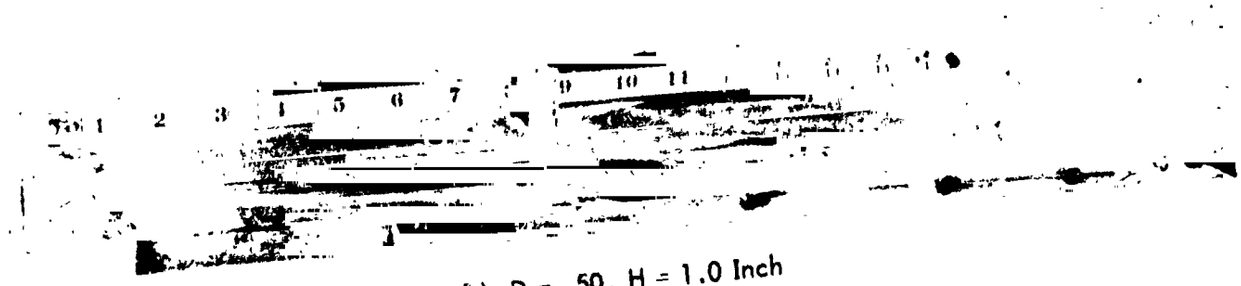

(b) D = .50, H = 1.0 Inch

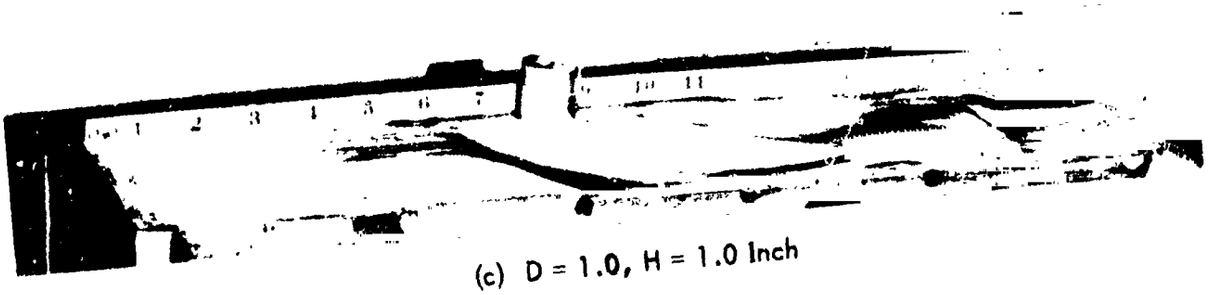

(c) D = 1.0, H = 1.0 Inch

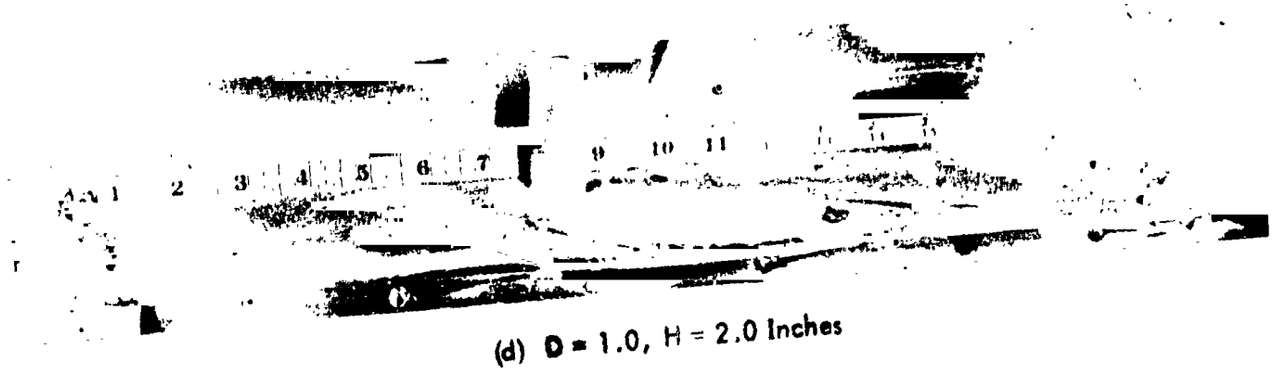

(d) D = 1.0, H = 2.0 Inches

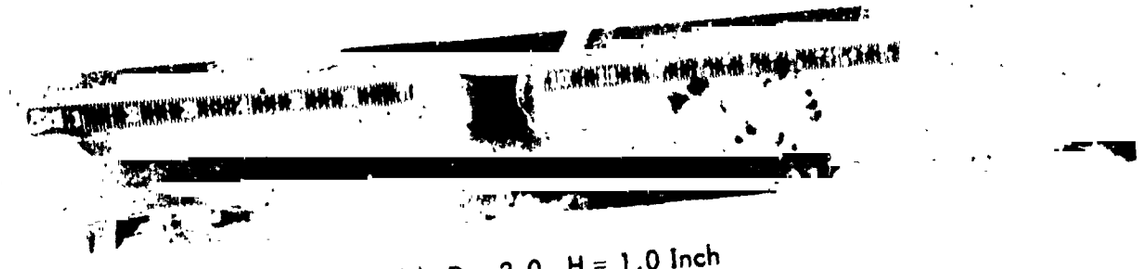

(e) D = 2.0, H = 1.0 Inch

Figure 17. Oil Flow Photographs of Cylindrical Protuberances at Mach 1.96

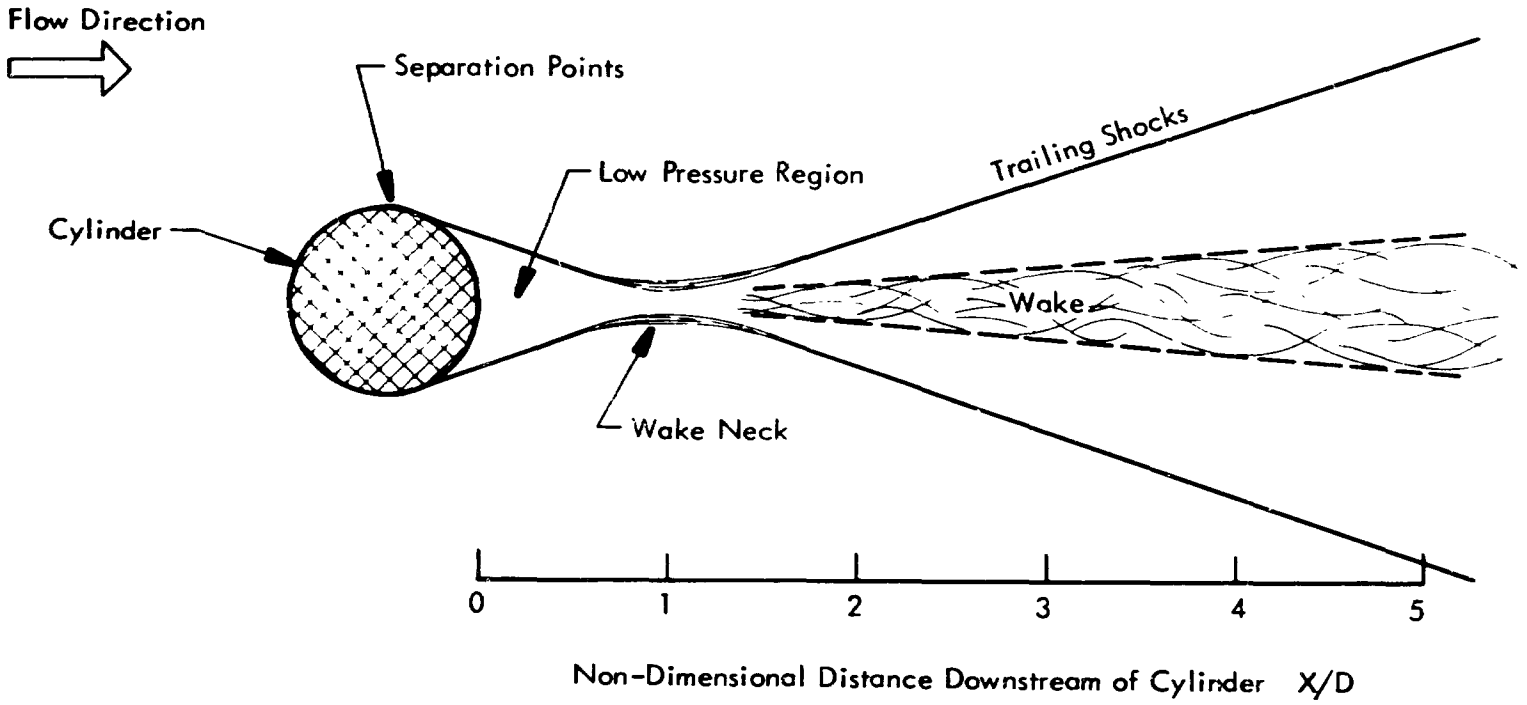

Figure 18. Composite Conception of Infinite Cylinder Wake Region

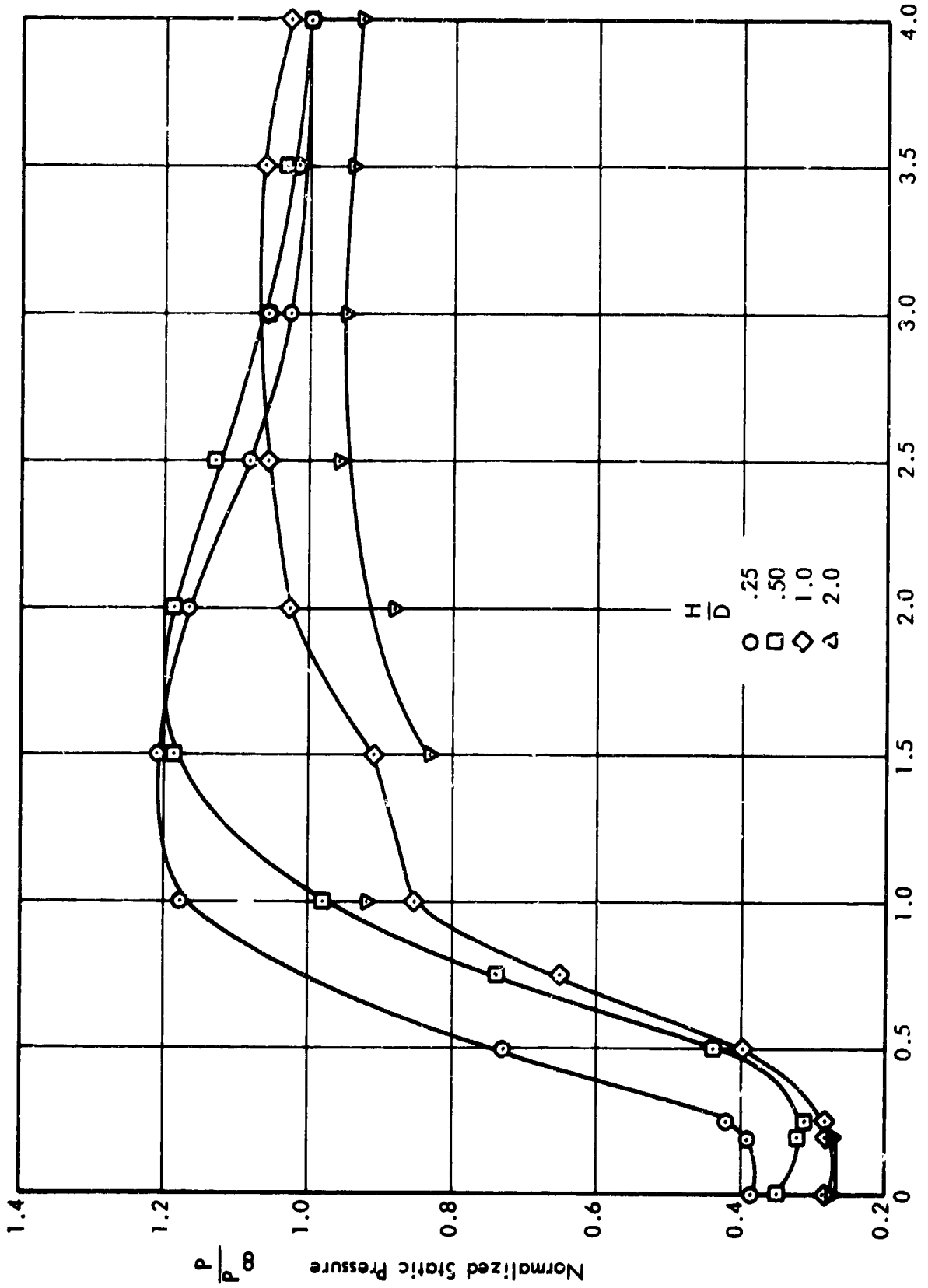

Figure 19. Downstream Centerline Pressure Profile for Cylindrical Protuberances at Mach 1.96

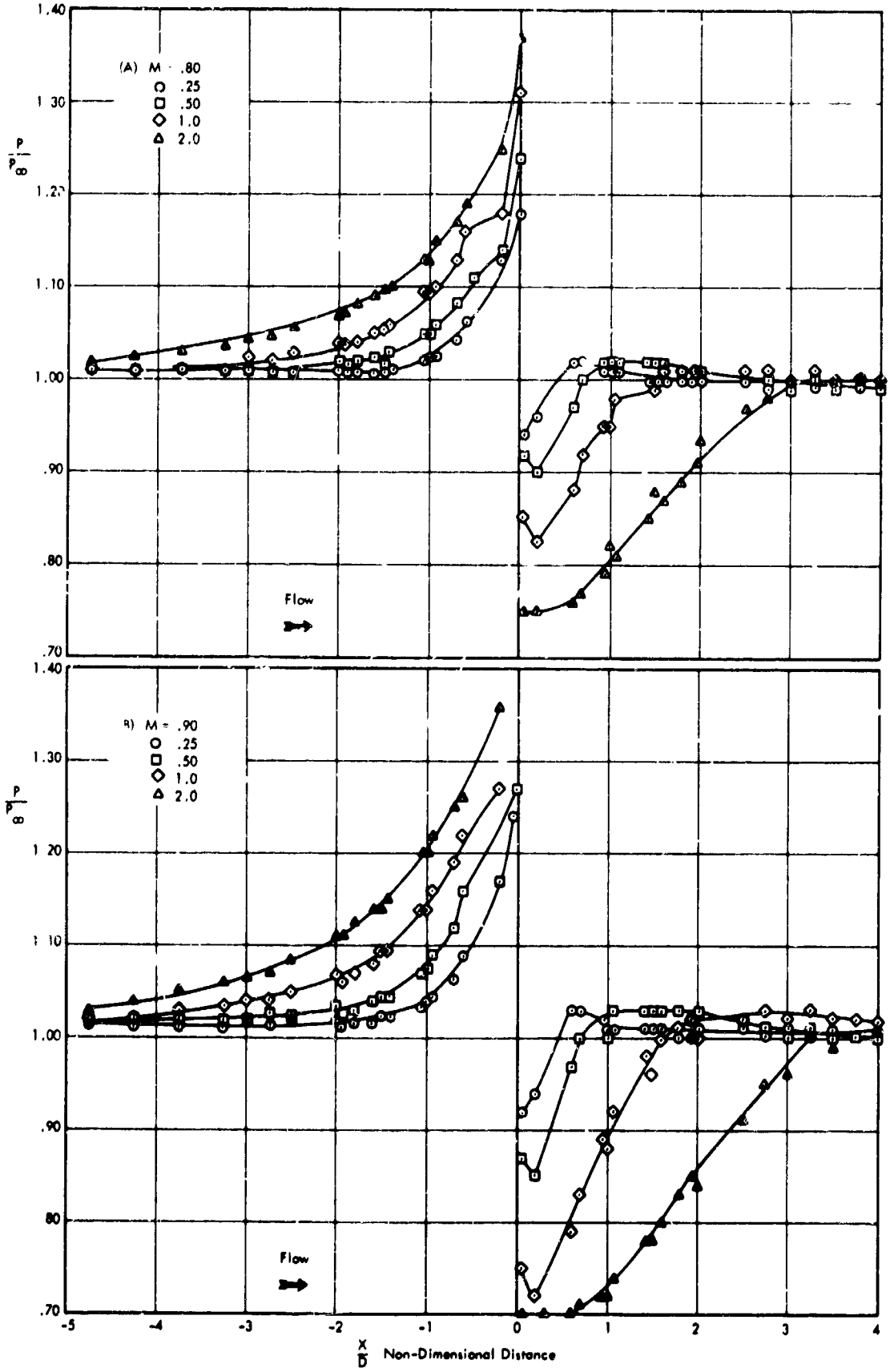

Figure 20. Upstream and Downstream Pressure Distribution of a 1-Inch Cylinder.

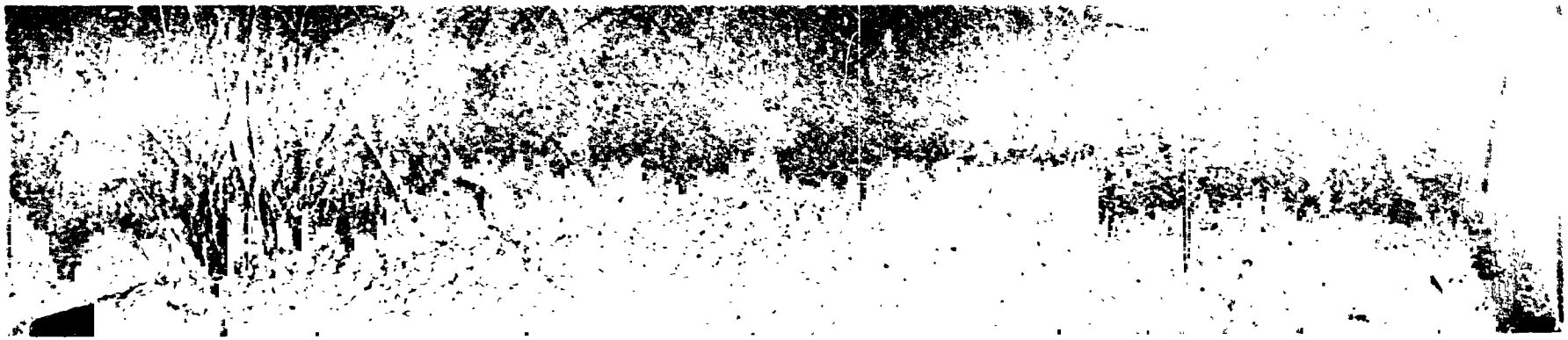

(a) Cylinder D = 1.0, H = 1.0 Inch, Forward Position

(b) RCS Motors

(c) APU

Figure 21. Shadowgraphs of Protuberances at Mach .80

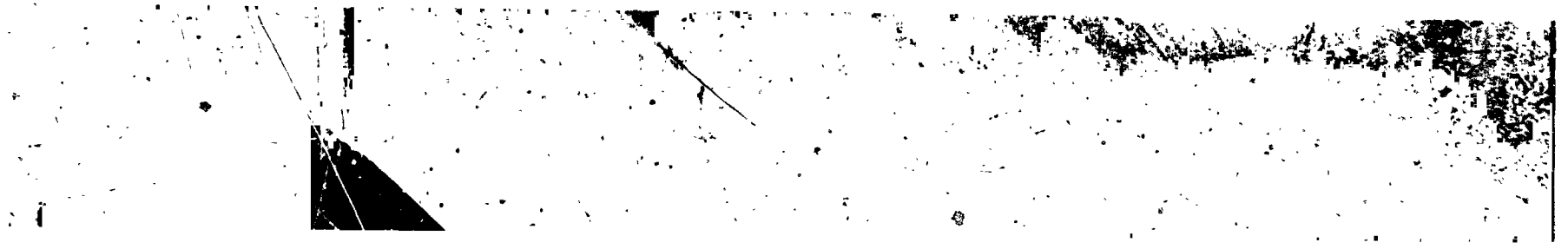

(a) Cylinder D = 1.0, H = 1.0 Inch

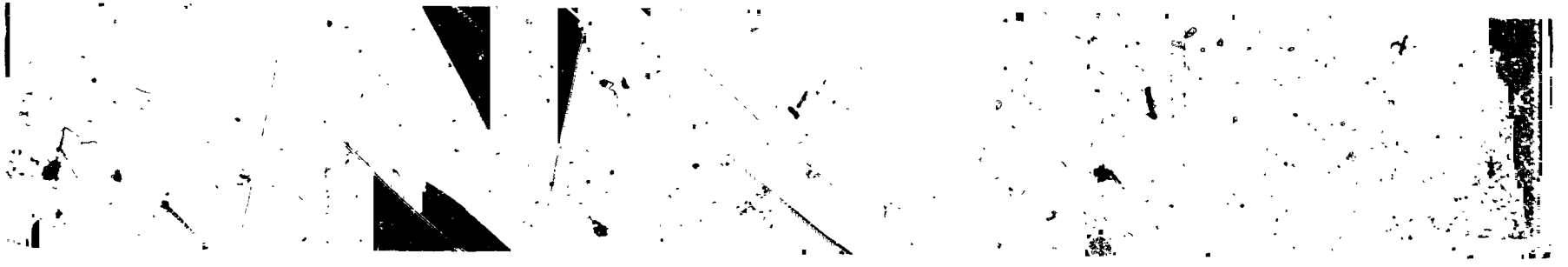

(b) RCS Motors

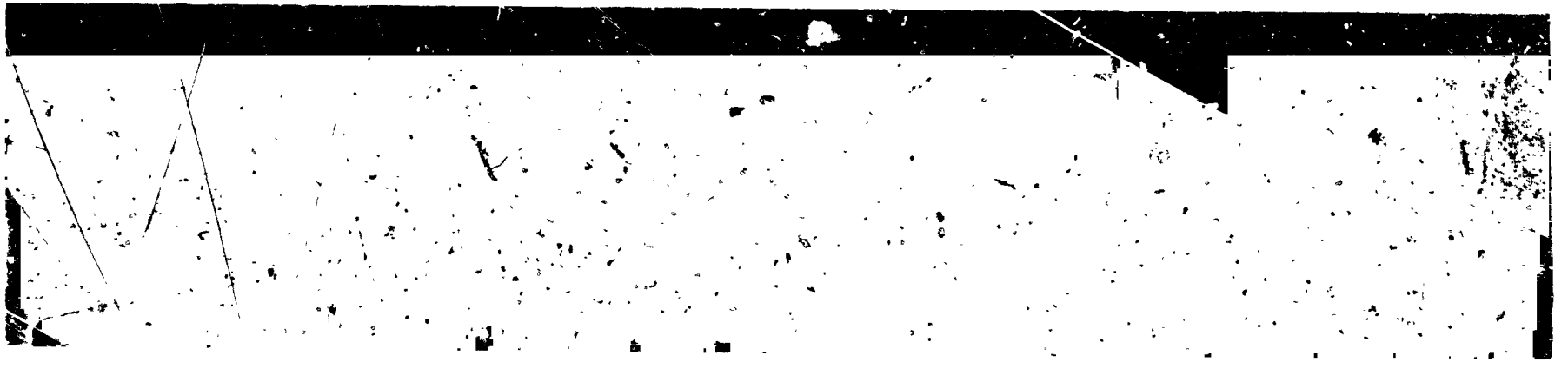

(c) APU

Figure 22. Shadowgraphs of Protuberances at Mach .90

(a) Cylinder D = 1.0, H = 1.0 Inch

(b) RCS Motor

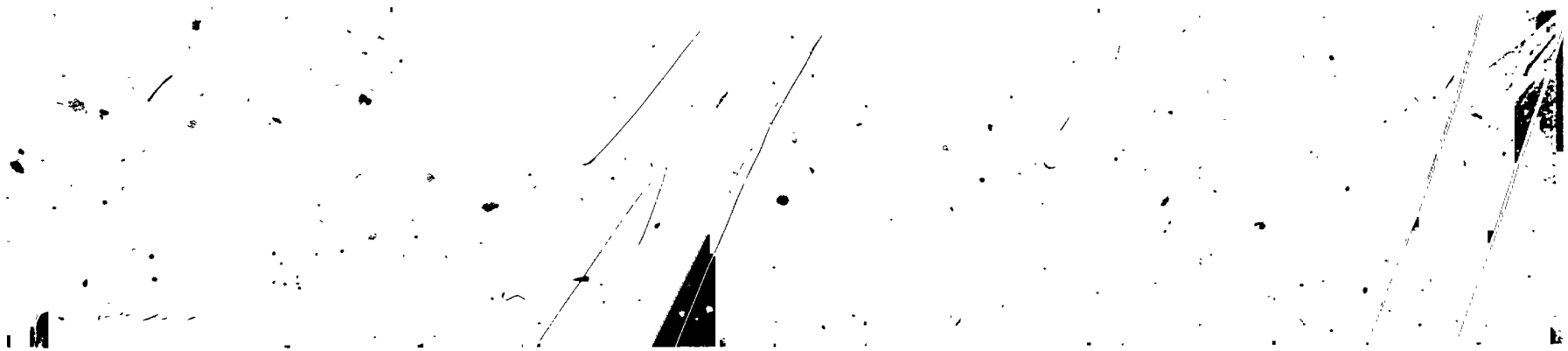

(c) APU

Figure 23. Shadowgraphs of Protuberances at M = 1.15

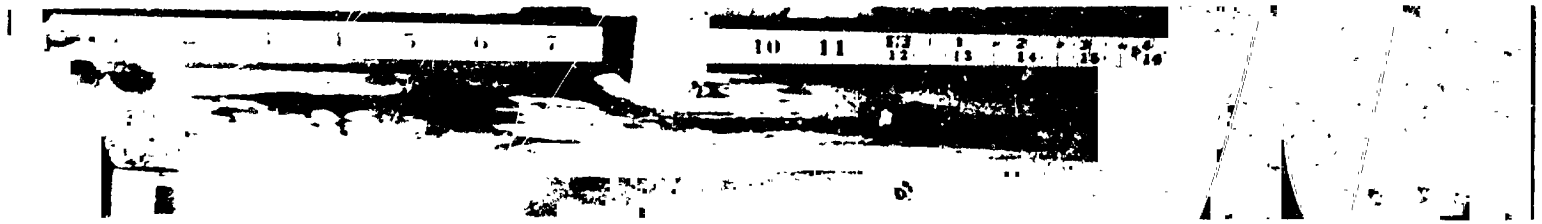

(a) M = .80

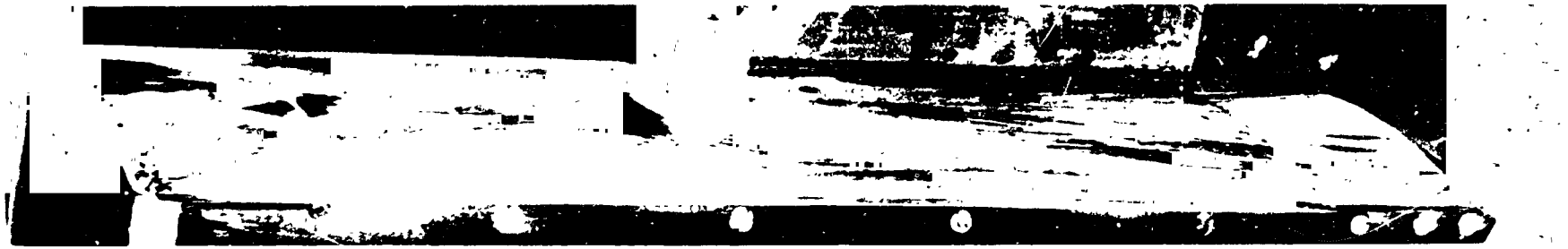

(b) M = .90

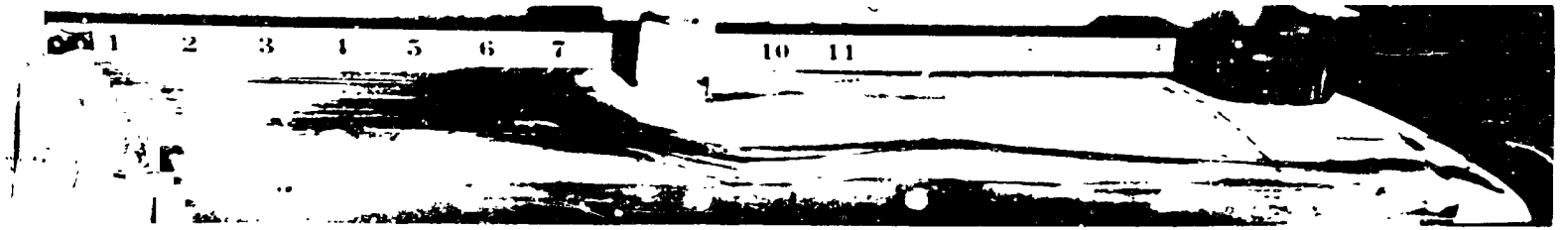

(c) M = 1.15

Figure 24. Oil Flow Photograph of a Cylinder Where H = 1.0, D = 1.0

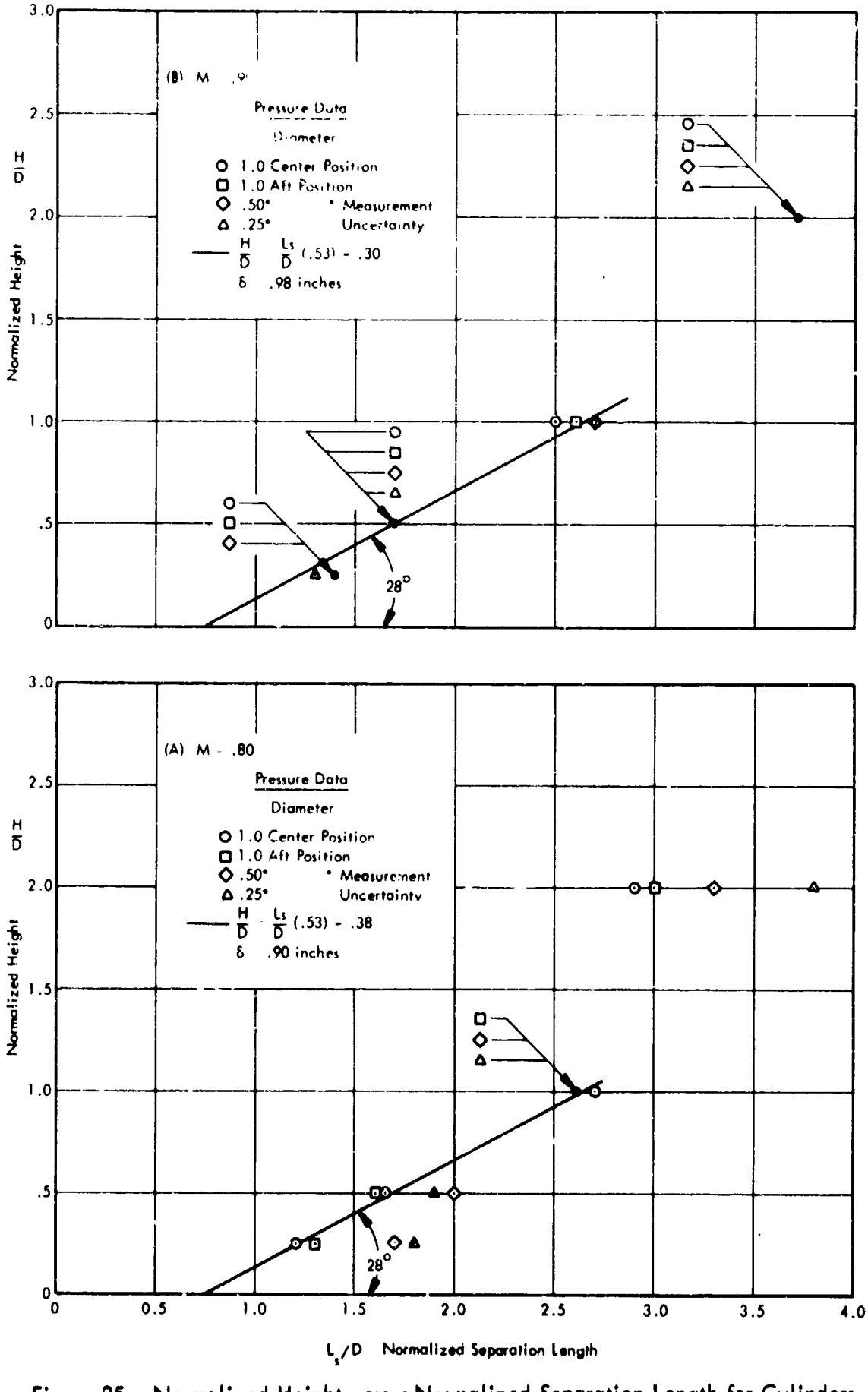

Figure 25. Normalized Height versus Normalized Separation Length for Cylinders.

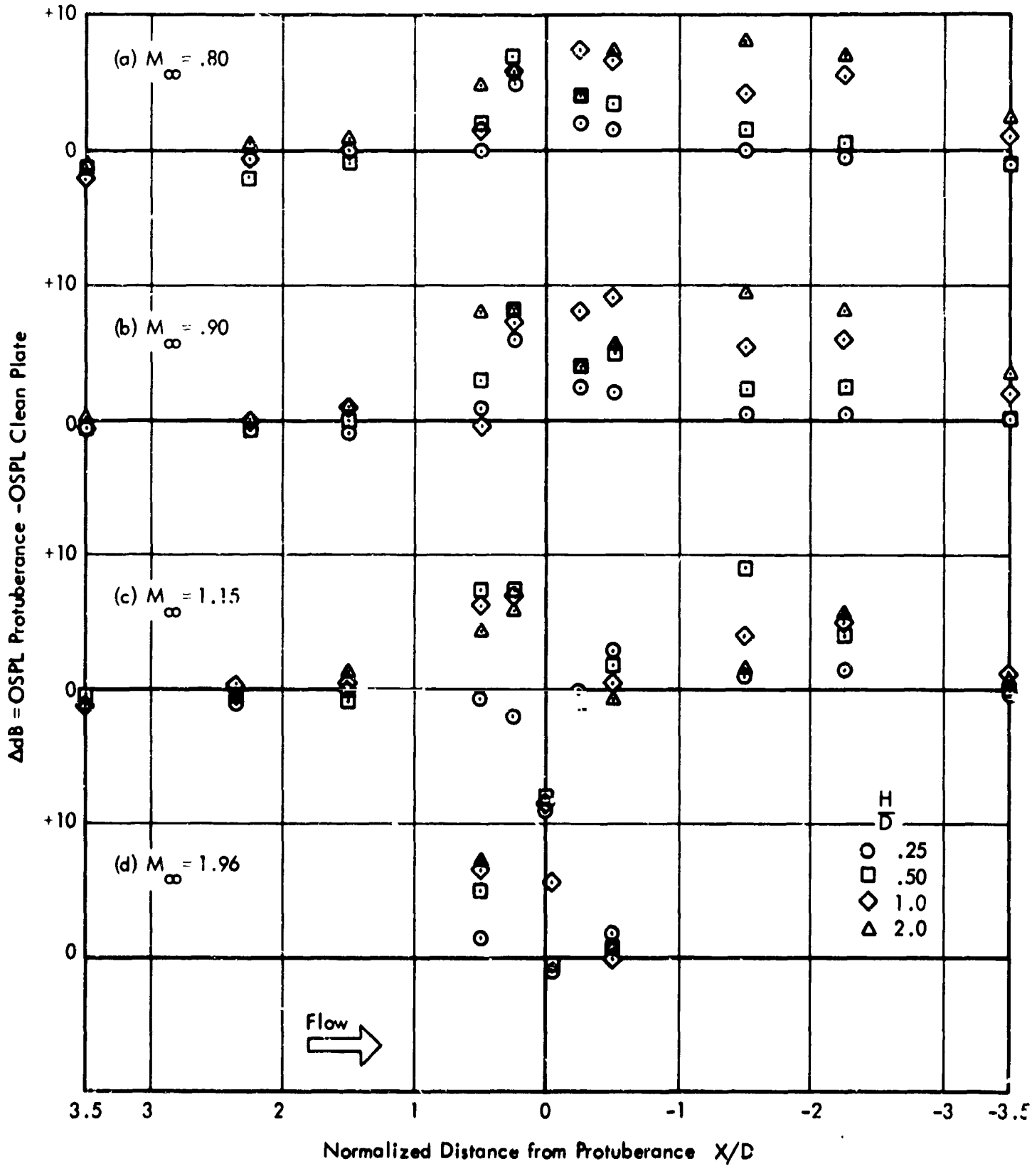

Figure 26. Centerline Fluctuating Pressure Profile Upstream and Downstream of Cylindrical Protuberances at M = .80, .90, 1.15, and 1.96.

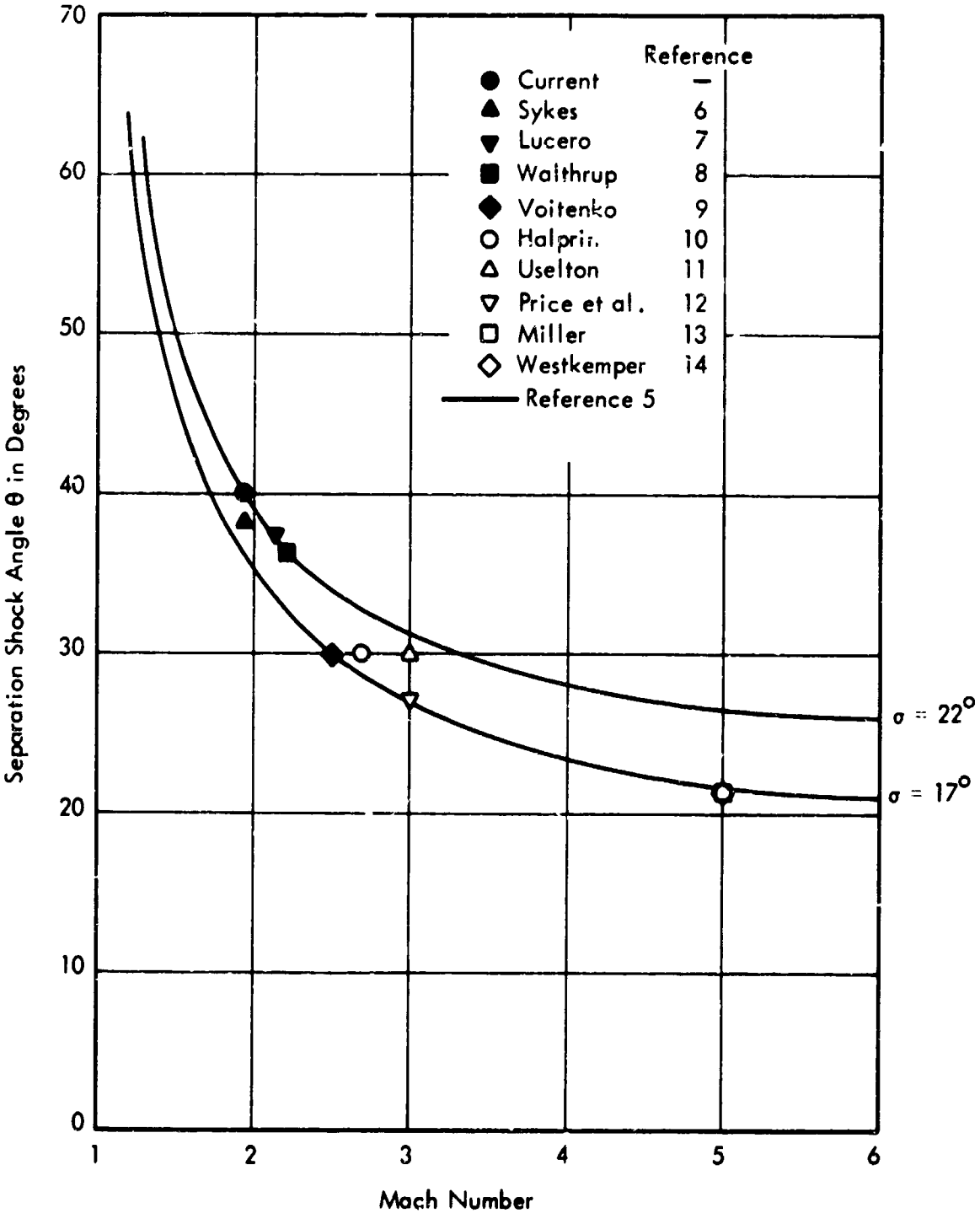

Figure 27. The Variation of Separation Shock Angle with Mach Number - Schlieren - Shadowgraph Data

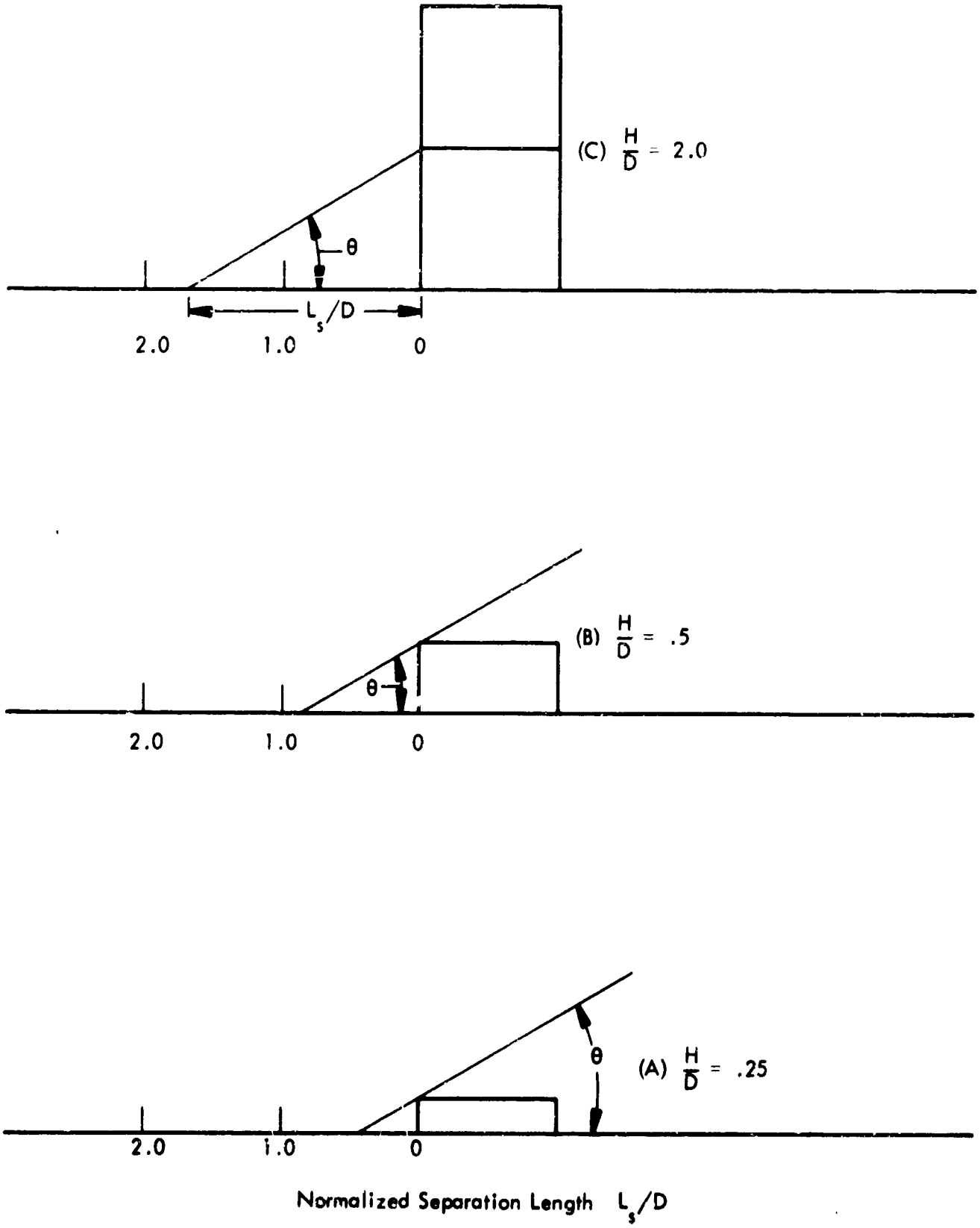

Figure 28. Idealized Model of Separation Upstream of A Cylindrical Protuberance at $M = 2.5$ and $\theta = 30^{\circ}$

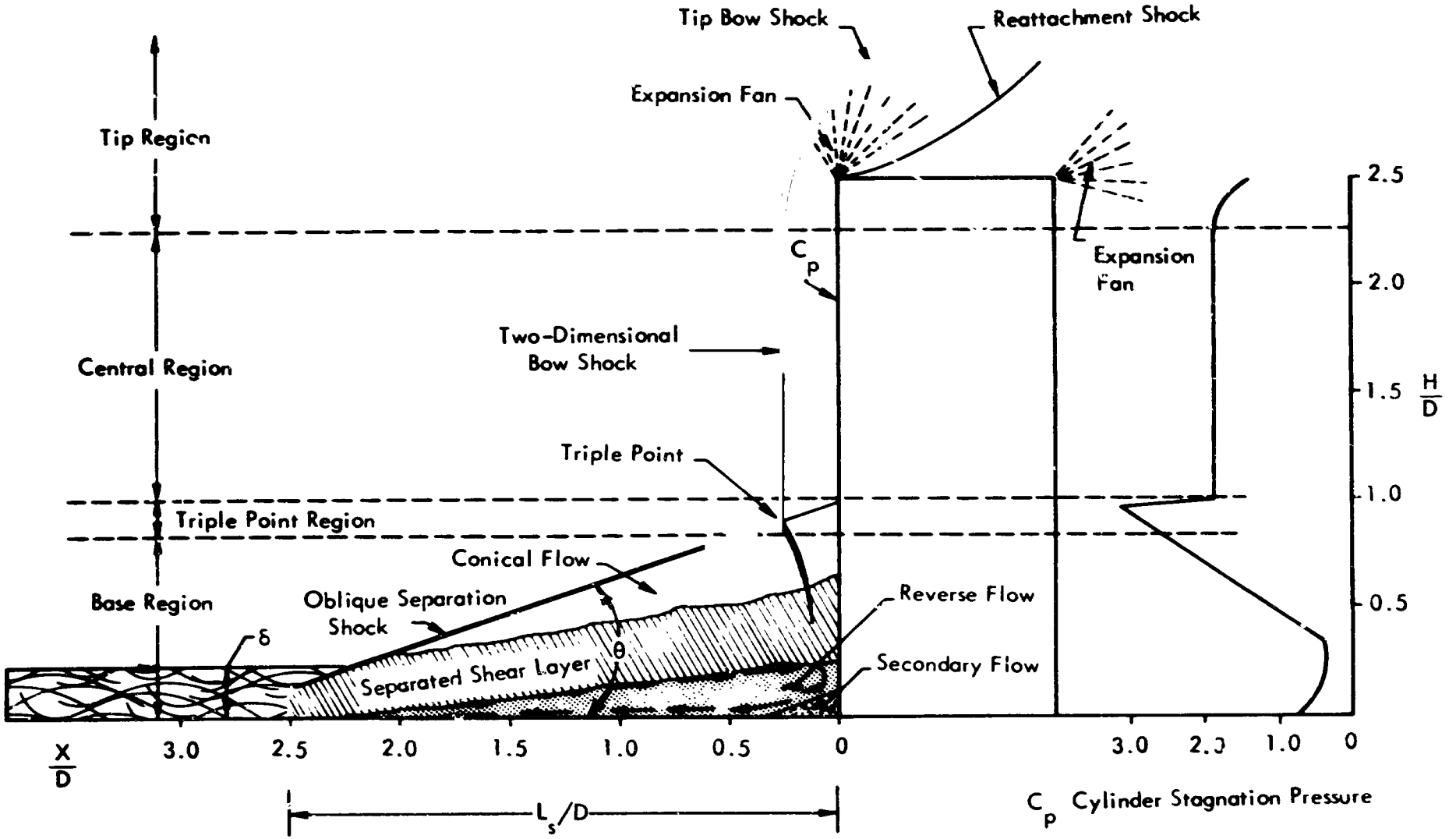

Figure 29. Correlation of Flow Fields and Stagnation Pressure (Miller Reference 13)

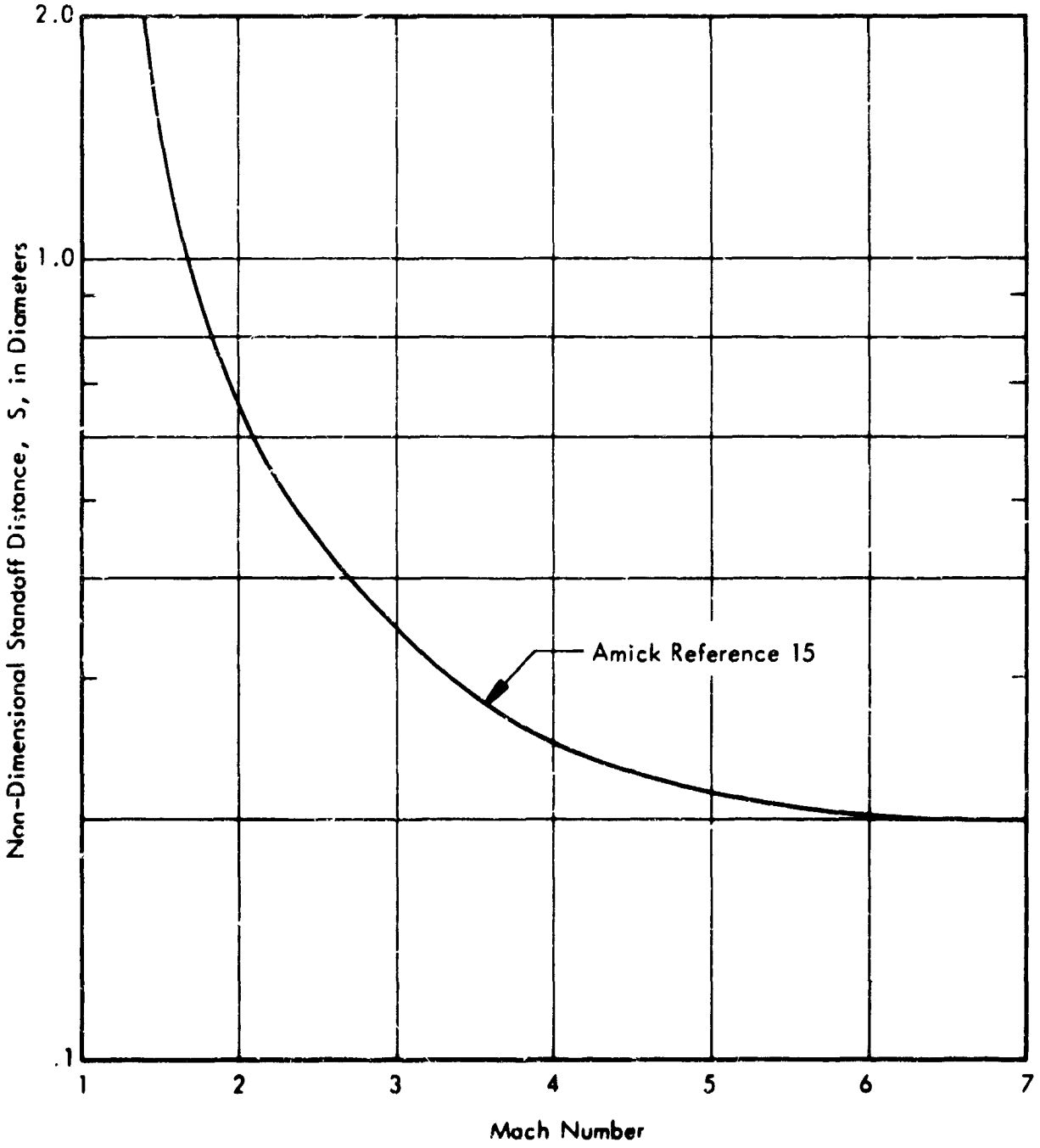

Figure 30. Bow Shock Standoff Distance versus Mach Number for an Infinite Cylinder

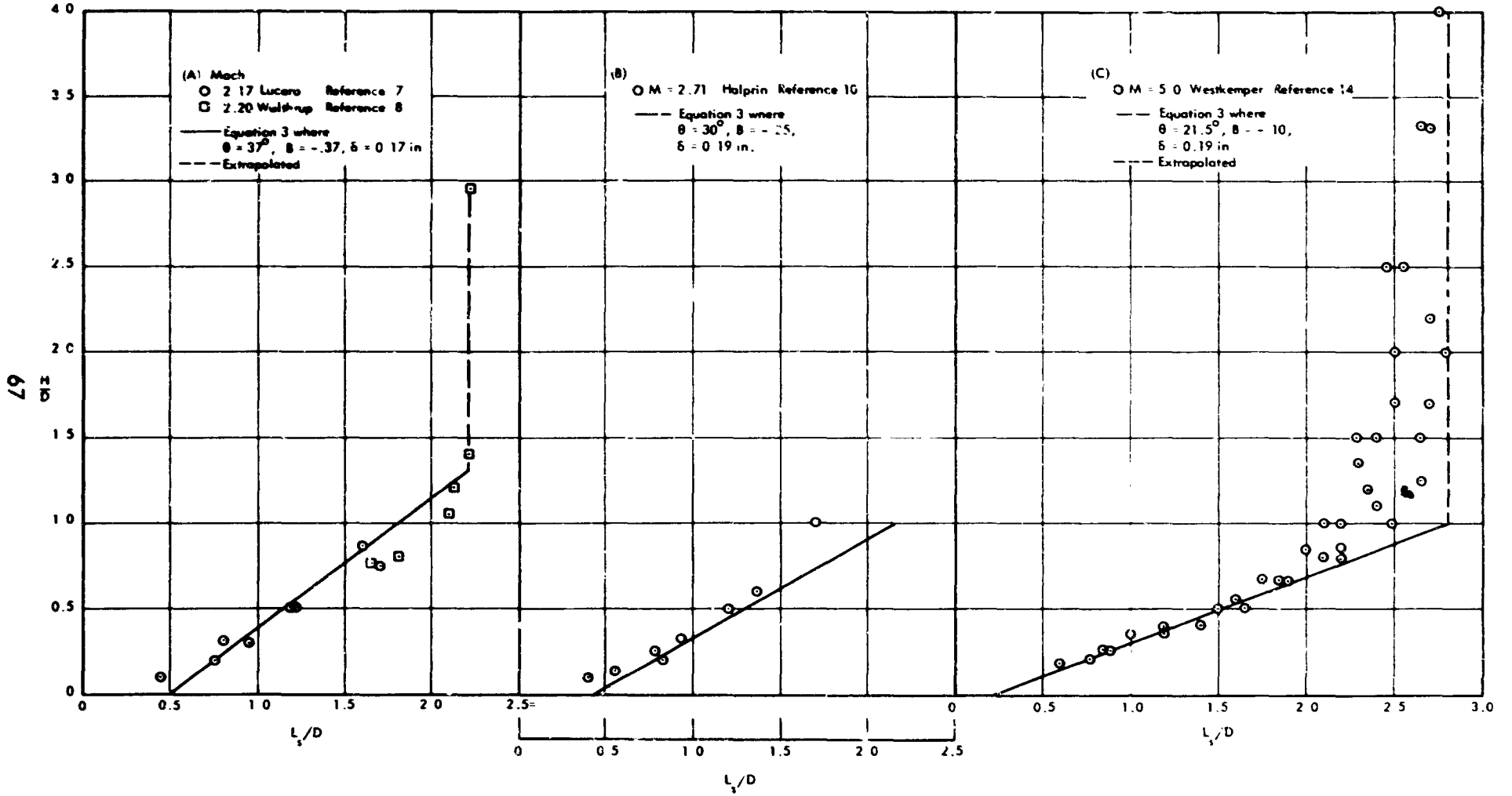

Figure 31. Correlation of Normalized Height with Normalized Separation Length For Cylindrical Protuberances at Mach 2.2, 2.7, and 5.0.

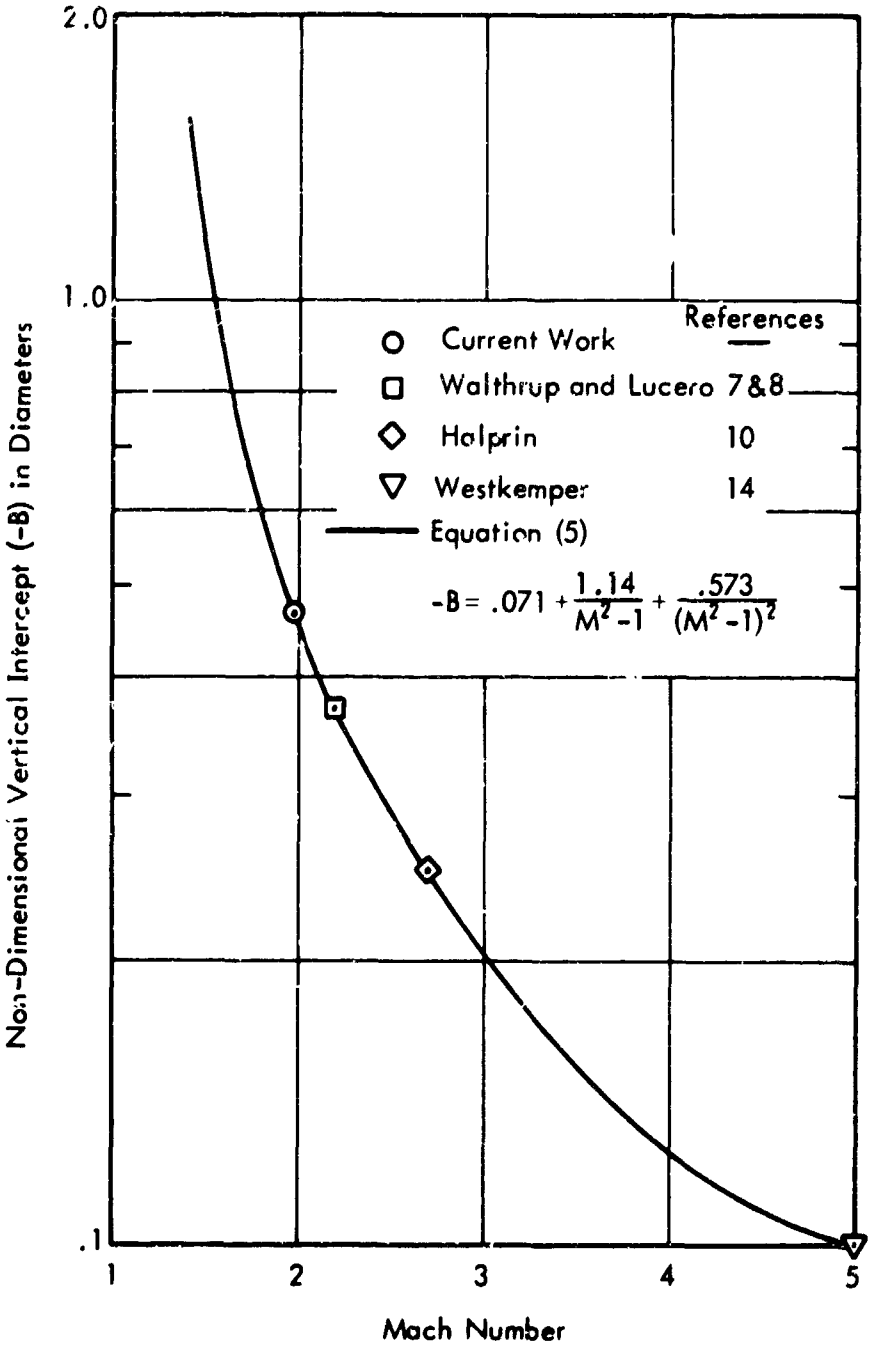

Figure 32. Variation of Vertical Intercept (-B) With Mach Number

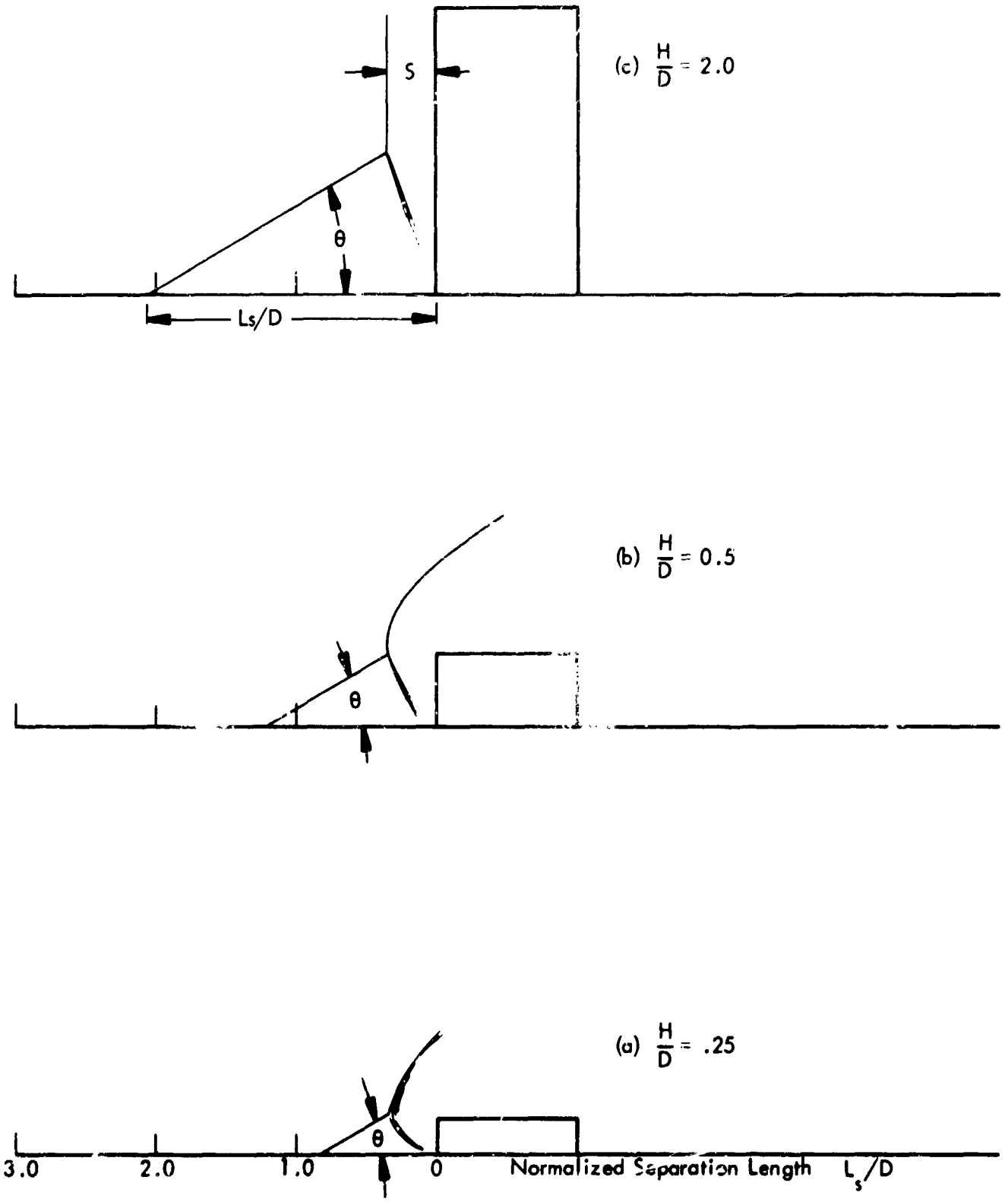

Figure 33. Modified idealized Model of Separation Upstream of a Cylindrical Protuberance at M = 2.5, θ = 30°

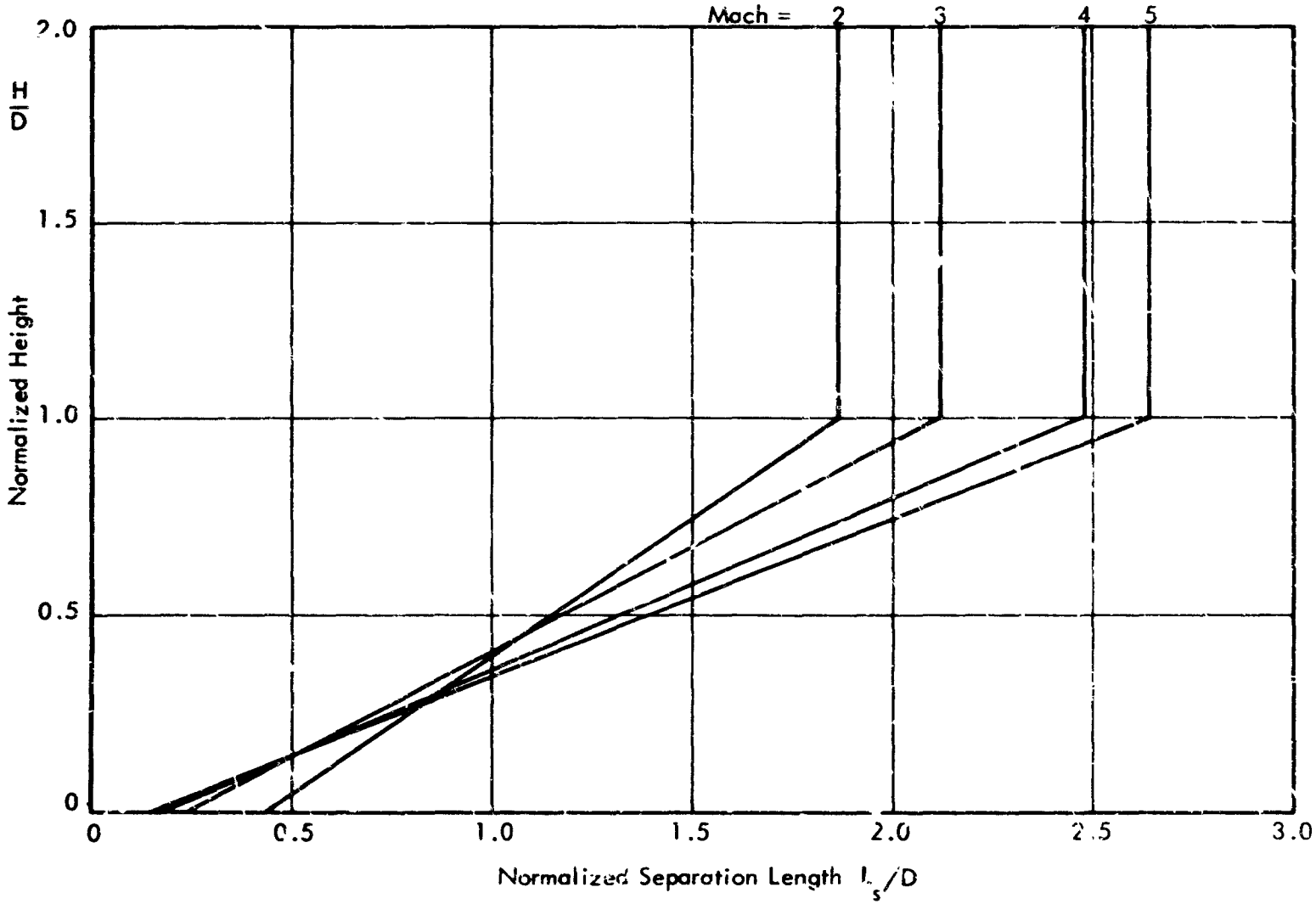

Figure 34. A Series of Curves Presenting Separation Length and Height as a Function of Mach Number

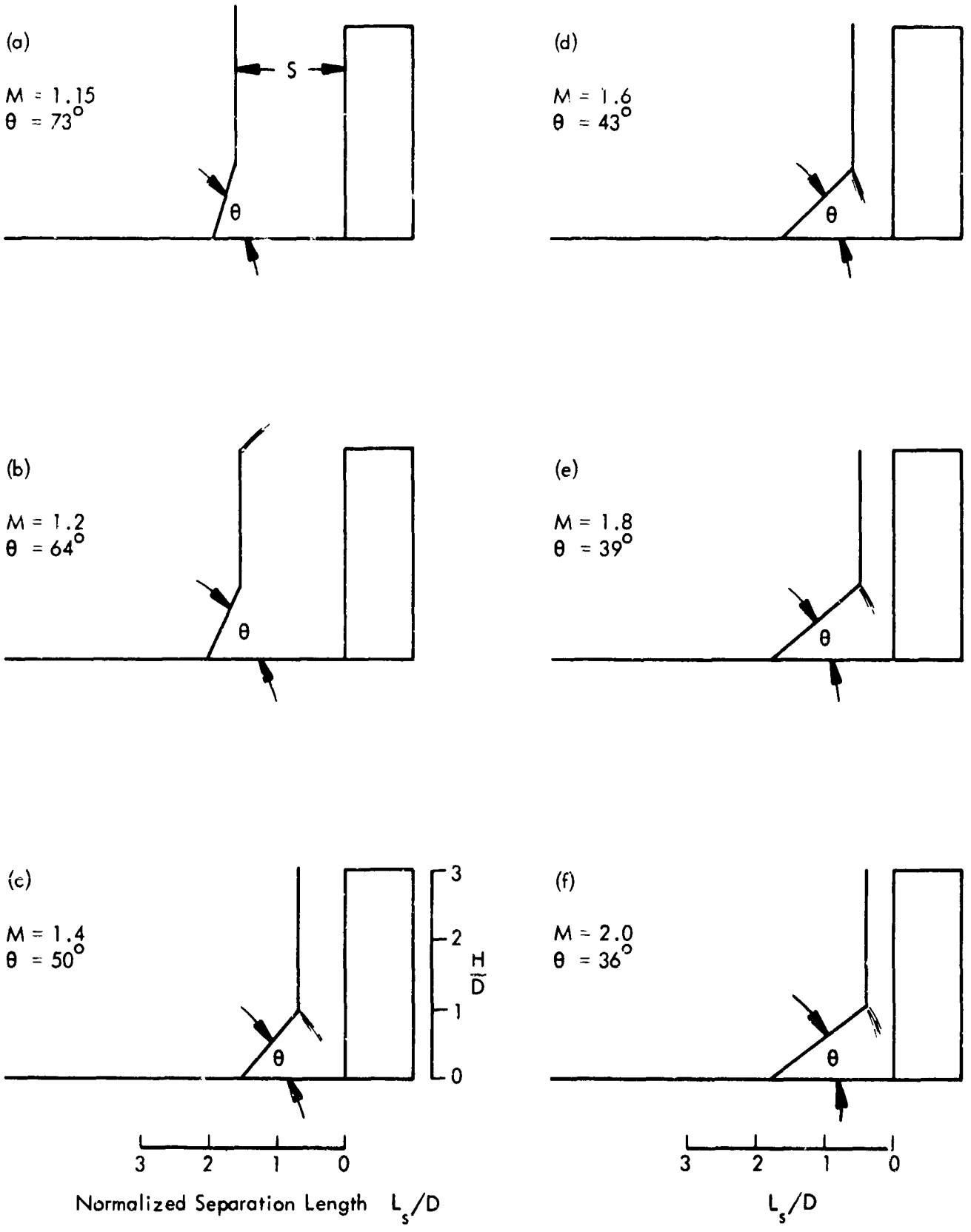

Figure 35. Expected Shock System Upstream of a Tall Protuberance at Low Supersonic Mach Numbers

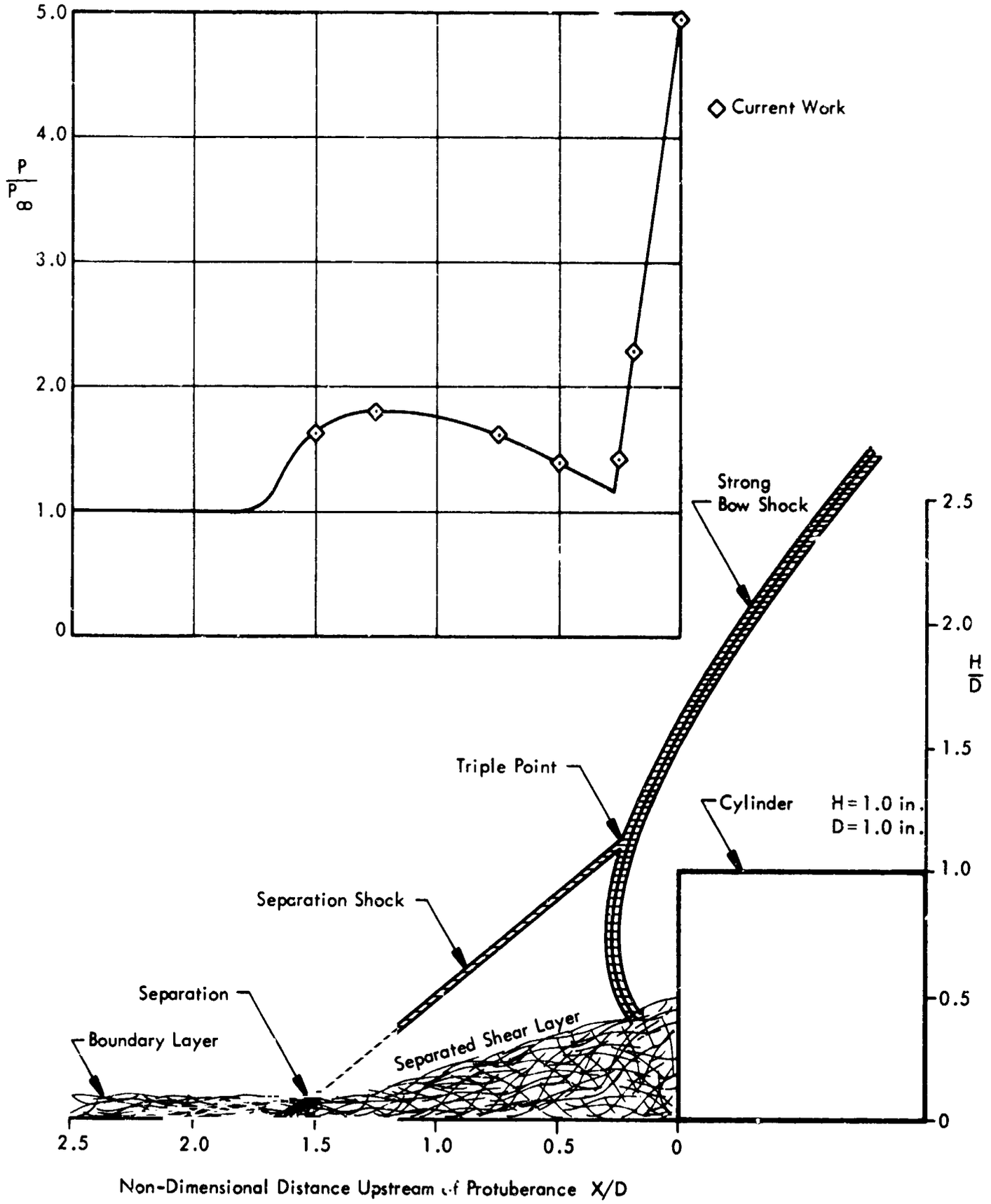

Figure 36. Comparison of Upstream Centerline Pressure Profile with the Lambda Shock System

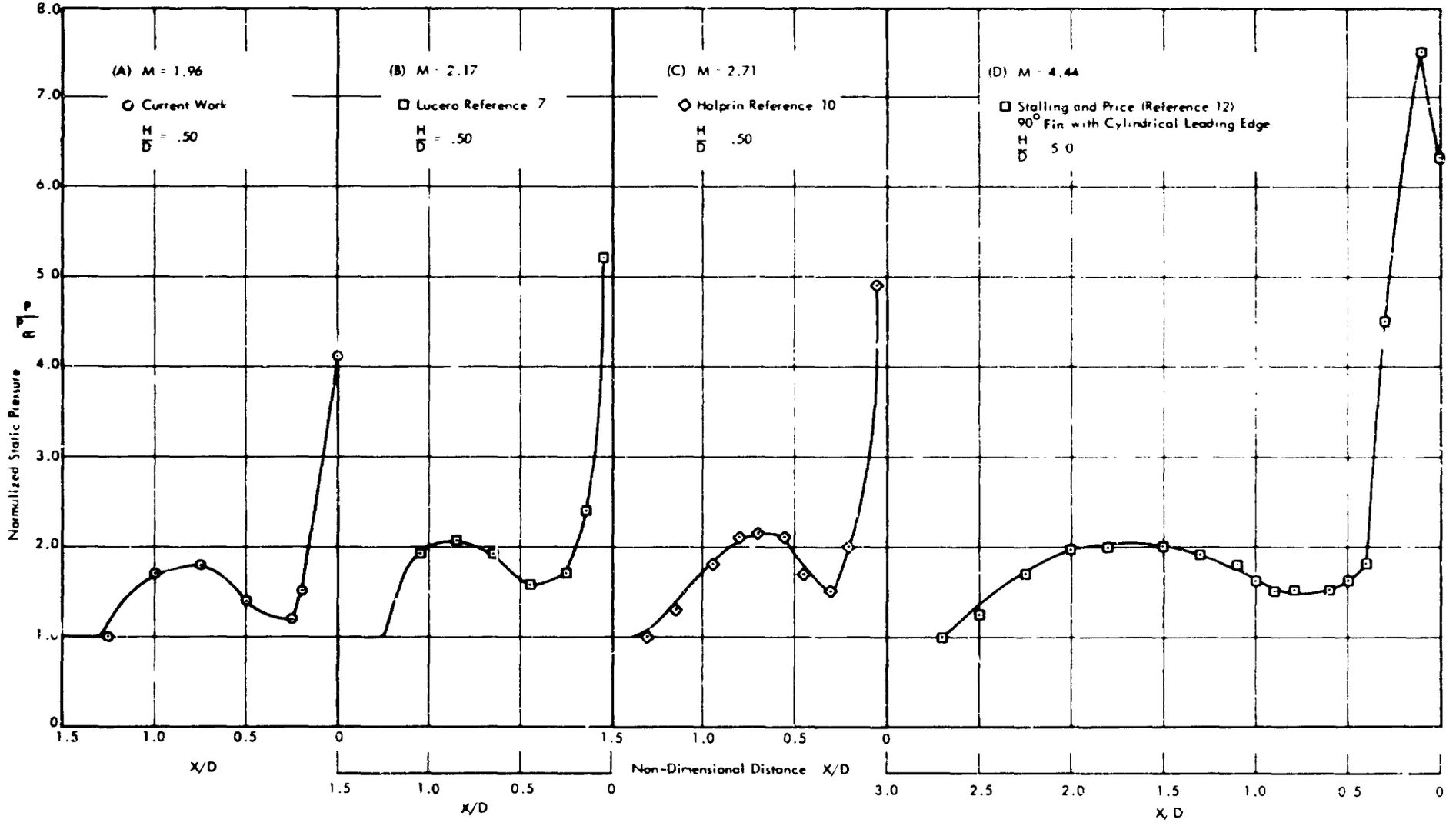

Figure 37 Upstream Centerline Pressure Profile for Cylindrical Protuberances

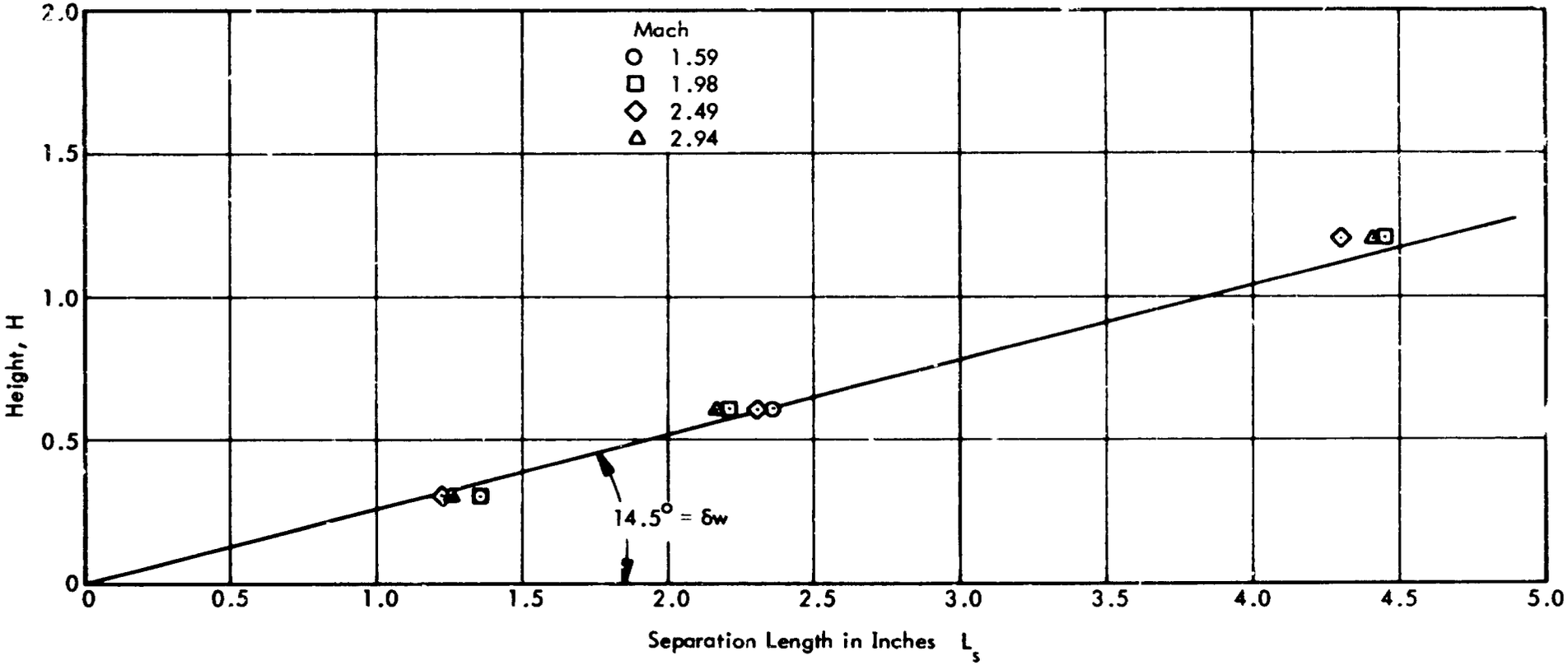

Figure 38. Correlation of Height and Separation Length for Two-Dimensional 90° Steps (Lowson Reference 17)

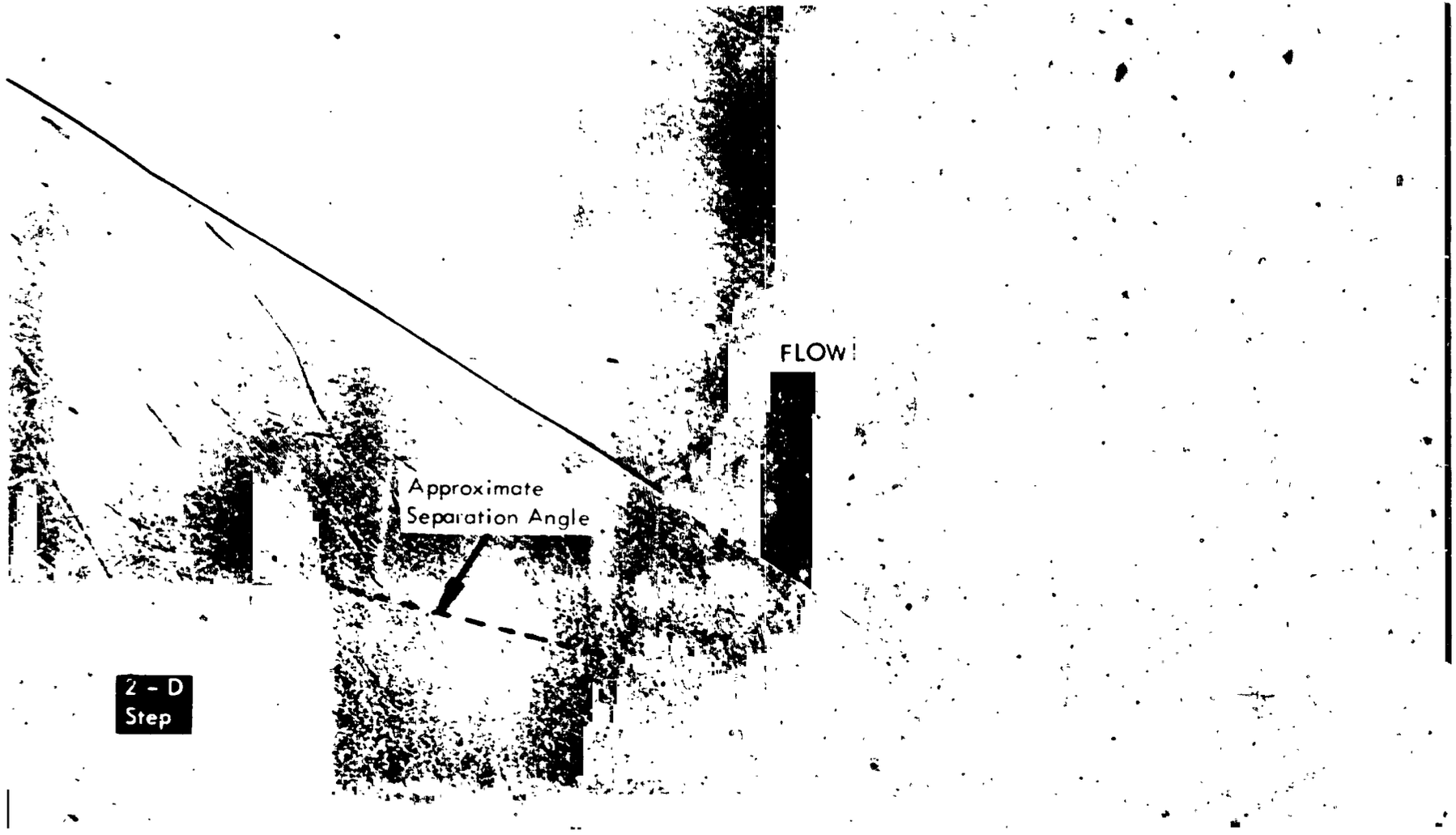

Figure 39. Photograph of Two-Dimensional Flow Showing Separation Upstream of a 90° Step. M = 2.49, Step Height = .6 Inch, Lowson (Reference 17)